A Geographically Weighted Regression Approach to Landslide Susceptibility Modeling

A Thesis
Presented in Partial Fulfillment of the Requirements for the
Degree of Master of Science
with a
Major in Geography
in the
College of Graduate Studies
University of Idaho
by

Daniel T. Matsche

Major Professor: Karen Humes, Ph.D.
Committee Members: John Abatzoglou, Ph.D.; Raymond J. Dezzani, Ph.D.
Department Administrator: Mickey Gunter, Ph.D.

May 2017

AUTHORIZATION TO SUBMIT THESIS

This thesis of Daniel T. Matsche, submitted for the degree of Master of Science with a Major in Geography and titled "A Geographically Weighted Regression Approach to Landslide Susceptibility Modeling," has been reviewed in final form. Permission, as indicated by the signatures and dates below, is now granted to submit final copies to the College of Graduate Studies for approval.

Major Professor: _____ Date: _____
Karen Humes, Ph.D.

Committee Members: _____ Date: _____
John Abatzoglou, Ph.D.

_____ Date: _____
Raymond J. Dezzani, Ph.D.

Department
Administrator: _____ Date: _____
Mickey Gunter, Ph.D.

ABSTRACT

Landslide activity in Oregon causes more than $1 billion in property damage every year, and has resulted in several casualties over the past decades. The steep topography of the region, high-intensity precipitation events during the winter months, and easily weathered parent material, contribute to frequent slope failures in western Oregon. This study conducted a statistical landslide susceptibility assessment to evaluate the effects of geologic, morphologic, physical, and anthropogenic factors on landslide occurrence. Slope, erosion potential, hydrologic soil classes, volcanic and sedimentary geologic material, aspect, and curvature were identified as important predictors. A comparative analysis of traditional logistic regression (LR) and geographically weighted logistic regression (GWLR) was completed for the study area. The regression results from the LR and GWLR models were compared based on AIC, percentage of deviance explained, and prediction accuracy. The outputs demonstrated that GWLR outperformed standard LR in all models. GWLR improved prediction accuracy by 6.2% compared to traditional LR.

ACKNOWLEDGEMENTS

First, I would like to thank my advisor, Dr. Karen Humes, for her relentless support, expertise, and dedication. Her guidance helped me during my thesis research and allowed me to gain a deep understanding of landslide analysis. Second, I would like to express my sincere gratitude to my committee members, Dr. Ray Dezzani and Dr. John Abatzoglou. Their immense knowledge made it possible for me to complete this analysis, and I am very thankful for their insightful comments on statistical modeling and climate science. Third, I would like to acknowledge Dr. Katherine Hegewisch. She helped me tremendously during my research and patiently taught me the fundamentals of MATLAB scripting. Finally, I wish to express my most sincere gratitude to the Northwest Climate Science Center for funding my research and giving me the opportunity to exchange information with scientists throughout the United States.

DEDICATION

This work is dedicated to my wife, Niccolette, for her continued support of my educational endeavors, and to my son, Felix, for making the final stages of my thesis research more interesting.

TABLE OF CONTENTS

LIST OF FIGURES

LIST OF TABLES

LIST OF EQUATIONS

CHAPTER 1: BACKGROUND AND RESEARCH QUESTIONS

It is estimated that landslides in the United States are responsible for 25 to 50 deaths annually, as well as damages over $1 billion (Sidle & Ochiai, 2006). With an increasing number of people residing and recreating in mountainous regions, the likelihood of loss of life and property continues to rise. There are numerous reasons why settlement occurs in potentially hazardous areas, including but not limited to, space constraints or a lack of financial mobility. Especially in developing nations, the latter is a problematic aspect that frequently results in widespread destruction of property, casualties, and severe personal hardship. Since mountains have always played an integral role in the development of culture and the creation of a viable economy (Price & Butt, 2000), it is not feasible to simply restrict settlement and the construction of infrastructure in mountainous terrain. In the Pacific Northwest, for instance, transportation routes are confined to valleys due to the topography of the region. They allow for the fast and efficient relocation of goods and services from inland locations to coastal cities. Road and railroad networks are frequently subject to landslide activity which not only endangers human life, but also causes substantial economic damage. Currently, there is no efficient alternative that avoids landslide prone areas completely. For that reason, communities in the Northwest and other mountainous parts of the world rely on accurate landslide predictors to enhance planning efforts and promote resilience.

Although landslides are accountable for considerable destruction and causalities, it is also reported that, in some cases, they are necessary agents providing positive effects for ecosystems and biodiversity (Geertsema & Pojar, 2007; Restrepo, et al., 2009). For instance, landslides are responsible for significant amounts of natural sediment and biomass in streams around the world (Sidle & Ochiai, 2006). Besides adding nutrients to stream systems, large woody debris can establish vital pools, encourage periphyton growth, a valuable food source for invertebrates, and provide stream shading and shelter to aquatic species. In systems free of human interference, landslide activity is controlled by natural processes. However, due to increasing anthropogenic influences, extent and frequency of slope movement has been altered and continues to change in a rapid way. Many of the physical factors that are associated with landslide activity, such as landcover change, rainfall intensity, or water-level fluctuation, for example, are directly and indirectly impacted by human activity. Therefore, it

is essential to integrate a large variety of physical components in landslide modeling efforts. The variance of model parameters across space make regional landslide susceptibility analysis challenging. Nonetheless, regional assessment is indispensable for effective, long-term planning. By incorporating future climate and land use projections, it would be possible to model landslide dynamics and evaluate changes in susceptibility on a temporal scale. This would allow land managers to implement zoning changes and adjust management strategies to reduce the effects of devastating slope failure events.

The main goal of this chapter is to convey necessary background knowledge about the types and processes of slope movement. It includes an overview of common terminology, information about landslide classification schemes, a comprehensive summary of factors influencing landslide susceptibility, a section providing context about the role of climate, and an outline of various modeling approaches currently available. In view of the complexity of this topic and variations in vocabulary among the disciplines involved in landslide research, it is essential to define the scope of this research. This study does not focus on the mechanical processes that govern slope failure. Instead, emphasis is put on the statistical methodology used to model the events and the effects that climate and other predictors have on the spatial distribution of landslide activity.

TERMINOLOGY

The process of slope failure in mountainous regions is a geomorphic phenomenon that has a long history of altering terrain by eroding and depositing sediment. Landslides are responsible for terrestrial diversity and present a powerful force that is shaping the landscape. There is a variety of terms that have been utilized to describe this process. Slope failure, mass movement, mass wasting, and landslide all define the redistribution of earth masses from areas of high to low topographic relief. For that reason, a landslide is a complex form of disturbance. Even though classifications and terminology can vary widely, in the United States, a landslide is defined as “the movement of a mass of rock, debris or earth down a slope” (Cruden D. M., 1991). Gravity is hereby the driving force which clearly distinguishes it from other forms of surface erosion where water or wind are the principal transport agents. During the process of shallow slope movement (depth <2 m), weaker, upper layers of slope

material separate from more stable bed rock. The underlying causes for this separation will be discussed later in the chapter. In the case of deep-seated landslides (depth >5 m), weathered or fractured bedrock itself can be found among the slide material (Sidle & Ochiai, 2006). While shallow landslides are very responsive to individual precipitation or snowmelt events, the responsiveness of deep-seated landslides to rainfall mainly dependents on the hydraulic properties of the bedrock and soil (Sidle & Ochiai, 2006).

LANDSLIDE TYPES

Besides a distinction between shallow and deep-seated slope failures, the colloquial term "landslide" encompasses several different movement types. Even though a variety of landslide classification systems have been proposed over the years (Sharpe, 1938; Keefer, 1984; Hutchinson, 1988), the most widely used scheme in the United States follows the system developed by Varnes (1978). It was adopted by the United States Geological Survey to explain different types of ground movement and is, for that reasons, utilized in this study. Table 1 illustrates the schematics of Varnes' original classification. An updated version of this organization, which encompasses additional parameters like water content and movement rates, is illustrated in Cruden and Varnes (1996). The updates significantly enhance the number of slope failure classification options available to researchers. None the less, it becomes important to note that each individual classification system has a particular applicability for approaching the topic of landslides (Sidle & Ochiai, 2006). Scope and research objectives must be considered before attempting the selection of a specific classification system.

Knowledge about parent material and type of movement are essential for classifying a landslide (Cruden & Varnes, 1996). Rock, debris, and earth describe commonly used types of material. Falling, toppling, sliding, spreading, flowing, or a combination thereof, categorize downslope movement of mass (Sidle & Ochiai, 2006). Consequently, combining material and movement results in a landslide classifications as proposed by Varnes (1978), namely "rock fall", "debris flow", or "earth slide", for example. Slides can be classified as "complex' when at least two different types of movement occur within a single slope failure (Varnes, 1978). Since various types of movement can predominate in different parts of the moving slope,

Cruden and Varnes (1996) recommend further sub-classification into “complex”, “composite”, “multiple”, “successive”, and “single”.

Table 1. Abbreviated Classification of Slope Movement (Varnes, 1978)

Type of movement		Type of material		
		Bedrock	Engineering Soils	
			Predominantly Coarse	Predominantly Fine
Falls		Rock fall	Debris fall	Earth fall
Topples		Rock topple	Debris topple	Earth topple
Slides	Rotational	Rock slide	Debris slide	Earth slide
	Translational			
Spreads		Rock spread	Debris spread	Earth spread
Flows		Rock flow	Debris flow	Earth flow
		(deep creep)	(soil creep)	(soil creep)
Complex (i.e., combinations of two or more types of movement)				

When incorporating temporal aspects into the classification scheme, complexity is enhanced further. The rate of movement of a slope failure can be highly variable. Landslides occur within seconds, or in the case of a creep, over months or even years. Cruden and Varnes (1996), therefore, propose a seven-class velocity scheme that ranges from 16mm/year to 5m/s and allows researchers to establish a correlation between velocity and damage probability. In general, the higher the velocity of a landslide, the greater the likelihood of loss of life and property destruction. Risk assessment can also be supplemented by knowledge about the size of a slide event, since large, moderate velocity movements are far less damaging than small, rapid failures (Cruden & Varnes, 1996).

Even though detailed descriptions and classifications of slope movement are helpful for engineers and geotechnical staff, Sidle and Ochiai (2006) caution that this complexity can be confusing to land managers. For assessing land management impacts and landslide risk, it is most important to focus on size, rate of movement, response to climate and seismic activity, as well as susceptibility to anthropogenic factors (Sidle & Ochiai, 2006). Researchers must be understand that each method of classification has certain limitations. This is demonstrated by a case study of the prehistoric Blackhawk landslide in the San Bernardino Mountains (Cruden

& Varnes, 1996). As discussed in the literature, it would be extremely challenging to assess water content, rate of movement, and other necessary parameters without a thorough investigation shortly after the event. In the case of prehistoric landslides or slope failures in remote locations that are discovered years after the event, proper reconstruction of important parameters may not be feasible. A simpler classification method might be better suited in these instances.

As mentioned earlier, after the introduction of Varnes' original 1978 classification scheme, only minor changes were attempted in subsequent years (Sidle & Ochiai, 2006). In the United States, government agencies and researchers appreciate the original classification for its simplicity and applicability to a variety of management situations. After careful consideration, it was decided to also apply Varnes' original 1978 classification scheme for the purpose of this study. Scope, objective, and audience make it the most appropriate choice.

LANDSLIDE CAUSES

The causes of landslides are numerous but can be categorized into four classes: geologic, morphologic, physical, or anthropogenic (Cruden & Varnes, 1996). A distinction between natural and management-induced landslide causes becomes increasingly difficult in view of substantial anthropogenic changes imposed on the system. Seemingly natural events like precipitation patterns, are progressively influenced by anthropogenic forcing. This denotes that warming global temperatures alter the frequency and intensity of precipitation events. It is, therefore, challenging to establish a distinct classification of influencing factors. Overlap, as well as some level of uncertainty in the classification is inevitable.

Although a landslide can have several different causes, there can only be one trigger that initiates the slope movement (Wieczorek, 1996). Triggers are described as an "external stimulus…that causes a near-immediate response in the form of a landslide by rapidly increasing the stresses or by reducing the strength of slope materials" (Wieczorek, 1996). A list of landslide causes, is for that reason, also a comprehensive list of possible landslide triggers. The question of landslide occurrence depends heavily on other causal factors that simultaneously weaken a slope. In most instances, slope failure transpires after an interplay of several unfavorable conditions. Slopes that have been previously weakened by intensive

logging or bank cutting may be more susceptible to triggers than heavily vegetated hillsides with excellent drainage properties.

An array of landslide causes is discussed in the scientific literature, including but not limited to the geologic composition of parent materials, vegetation cover, or the lack thereof, rainfall and snowmelt, slope alterations during road construction, seismic activity, and excessive irrigation of hillsides (Sidle & Ochiai, 2006; Swanson & Swanston, 1977; Varnes, 1978; Wieczorek, 1996; Van Asch, Buma, & Van Beek, 1999). At the core, these factors encourage slope failure by either increasing shear stress, contributing to low strength, or reducing material strength (Cruden & Varnes, 1996). Natural or anthropogenic processes can remove lateral support, steepen slopes, impose surcharges, or weaken internal cohesion. Landslide causes have far-reaching implications for the physical properties of the soil mantle, and govern the interplay between forces that are acting to either initiate or resist slope failure (Swanston D. N., 1984).

Geologic Factors

The geologic composition of the slope material is of tremendous importance for landslide susceptibility and risk assessment. Contrasts in, permeability, strength, and weathering, can cause certain rock types to be more prone to landslide activity than others. Over time, parent material can have deteriorated through natural processes. The geologic properties of material have far-reaching implications for particle size distribution, as well as the degree and depth of weathering (Swanston D. N., 1984). Texture of the parent material governs cohesion and angle of internal friction (Swanston D. N., 1984). It plays a role in the relative stability of a slope. However, parameters like water holding capacity and the slope gradient also need to be considered for this assessment. In some cases, it is also possible to find terrain that is underlain by intrinsically weak slope material. Decomposed rocks, such as chemically weathered volcanic tuffs, schists, and serpentinites may possess lower natural strength (Cruden & Varnes, 1996). Due to variations in density, geologic materials have differing levels of relative strength, the ability to resist failure. Unfavorable locations of fault lines, orientation of bedding, or schistosity, for example, can further enhance landslide susceptibility (Cruden & Varnes, 1996).

In the Pacific Northwest, extensive research has established a relationship between geologic composition and landslide susceptibility (Swanston & Swanson, 1976; Swanson & Swanston, 1977; Swanston D. N., 1984). It is asserted that especially on the western side of the Cascade Mountains, humid, high-precipitation conditions stimulate chemical weathering and result in the transformation of volcaniclastic rocks to clays (Swanston D. N., 1984). The process is locally extensive and signifies that hillsides underlain by fine-grained sedimentary, weathered volcaniclastic, and serpentine-rich rocks, as well as glacio-lacustrine silts and clays are susceptible to slope failures if sufficient water input is available (Swanston & Swanson, 1976). Thus, these parent materials are less prone to landsliding on the semi-arid, eastern side of the Cascades (Swanston D. N., 1984).

Geologic maps are frequently used in developing nations for susceptibility analysis because of their broad availability (Sidle & Ochiai, 2006). However, since the strength of bedrock is region specific and driven by the extent of weathering, as well as the amount of water infiltration, the utility of solely geologic hazard models is problematic. Yet, knowledge about the parent material is certainly useful as a general indicator of relative soil stability (Swanston D. N., 1984).

Morphologic Factors

Morphologic causes of landslide activity include natural processes such as tectonic uplifting, glacial rebound, various forms of erosion at the toe of a slope, deposition of material at the crest, or vegetation removal through forest fires, insects, and drought (Cruden & Varnes, 1996). By altering slope gradients through tectonic activity, hillsides may steepen and form fractures. This condition is widespread in the Cascade Range where a chain of volcanoes, extending from British Columbia to northern California, has created substantial slope angles. Oversteepened valleys are also frequently formed by glacial movements that cut deep into the local bedrock, or by rivers and streams that remove material through fluvial processes (Varnes, 1978). Steep gradients increase shear stress, and resulting fractures allow fluids to infiltrate a hillside at a much faster rate. Intrusion of snowmelt and precipitation enhance pore-water pressure and expedite weathering (Cruden & Varnes, 1996; Swanson & Swanston, 1977). The lateral pressure created by seepage may intensify when temperature

driven swelling and freezing occurs within the slope (Varnes, 1978). The combination of mild temperatures and high water content expedites the rate of chemical weathering. It can alter the overall cohesion strength of bedrock. This phenomenon is particularly prevalent on the western slopes of the Cascades where a transformation of minerals to clays and clay-size particles due to humid conditions is evident (Swanston D. N., 1984).

With the addition of material onto slopes through glaciers, volcanic activity, or wind, significant changes in terms of weight, length, and height may alter overall stability. Rapid modifications of the weight distribution can cause slope failures, or impact the resilience to other triggering mechanisms. Retreating and thinning glaciers in the Cascades left behind large amounts of unconsolidated deposits that are easily mobilized (O'Connor, Hardison, & Costa, 2001). This material can be rapidly redistributed through processes like debris flows, glacial outburst floods, or moraine-dammed lake failures, for instance, resulting in a surcharge of material onto slopes, thus enhancing sheer stress. Added weight from vegetation, snowpack, or intense rainfall causes similar outcomes (Varnes, 1978).

When material is removed, particularly at the toe of a slope, stability is also impaired. In terms of morphologic forms of removal, Cruden and Varnes (1996) list erosion by waves, glaciers, and other fluvial processes. During flooding events, the hydrologic force of water can erode underlying support and trigger a slope failure. Subterranean erosion, the removal of soluble material, can have similar effects on cohesion strength (Varnes, 1978). In a case study focusing on the Zentoku landslide in Japan, a link between high intensity rainfall and underground erosion was established (Hong, Yu, & Wu, 2011). For shear zones between five and twenty meters, subterranean erosion was found to be most influential (Hong, Yu, & Wu, 2011). A temporary surge in groundwater flow lead to a removal of material in the shallow and medium depths which facilitated failure.

Physical Factors

One of the most important physical causes of slope movement involve the role of water through intense rainfall, rapid snowmelt, or changes in water level near rivers, lakes, or reservoirs (Cruden & Varnes, 1996). Precipitation and varying ground-water levels, among others, result in slope saturation which weakens hillsides and increases landslide risk. Rapid

infiltration of rain water temporarily raises pore pressure, and the additional weight of the water increases the load on a potentially unstable slope. Piezometric levels control weight and the development of positive pore pressure which reduces the overall resistance of the soil to sliding (Swanson & Swanston, 1977). Many of these hydrologic landslide triggers are correlated to large-scale climatologic processes that transform our planet in a rapid way. Especially the effects of shifting precipitation patterns, in terms of magnitude and frequency, have far-reaching consequences for the distribution of landslides (Dhakal & Sidle, 2004). In addition to intense rainfall events, prolonged periods of above-average precipitation can saturate hillsides and result in slope failure (Cardinali, et al., 2006). An extreme precipitation event, accounting for 21% of the annual mean rainfall in parts of the Czech Republic in July 1997, triggered a series of landslides that caused widespread destruction of buildings, transportation networks, and reservoirs (Krejčí, et al., 2002).

Precipitation thresholds have been extensively studied and present an important aspect of landslide susceptibly analysis (Dhakal & Sidle, 2004; Van Asch, Buma, & Van Beek, 1999; Caine, 1980; Guzzetti, Peruccacci, Rossi, & Stark, 2007; Glade, Crozier, & Smith, 2000; Dahal & Hasegawa, 2008; Crozier, 1999). Generally, after a certain threshold of cumulative precipitation and maximum hourly rainfall intensity is exceeded, slope failure occurs (Sidle & Ochiai, 2006). It is extremely difficult to establish overarching thresholds for the level of saturation. Thresholds are region specific and vary based on geologic parent material, vegetation cover, and slope drainage capabilities (Van Asch, Buma, & Van Beek, 1999). Furthermore, saturation resulting from a combination of water inputs, such as snowmelt and intense rain, can cause failure earlier since the total amount of water imposed on the hillside is much higher. As mentioned before, in cases where fractures within the soil mantle and bedrock are present, it is much easier for water to infiltrate deep into the hillside (Sidle & Ochiai, 2006). Consequently, pore pressure is increased. The total amount of moisture that can be facilitated by slopes depends on the water-holding capacity which is influenced by antecedent soil moisture and soil texture (Sidle & Ochiai, 2006).

Additionally, the freezing and thawing of moisture has a number of adverse implications for slope stability. First, this seasonal process promotes freeze-and-thaw weathering and causes a contraction or expansion of the slope material (Cruden & Varnes, 1996). As a result, cracks are formed that allow water to flow deep into the hillside. Second,

steep terrain that receives its cohesion from ice is negatively affected when thawing occurs. Especially the melting of high-elevation permafrost reduces rock stability and enhances landslide activity (Stoffel, Tiranti, & Huggel, 2014). In particular, dry creep events could increase (Sidle & Ochiai, 2006).

Other physical causes that have been linked to landslide activity include earthquakes and volcanic eruptions. Shaking of the ground may trigger mass movements in hillsides that have been weakened by other natural or anthropogenic processes. Earthquakes increase transitory stresses that alter the local stress field within a slope (Cruden & Varnes, 1996). In some cases, it has also been reported that a reduction in shear strength can result from seismic activity (Varnes, 1978). When frequent earthquakes occur in an area, progressive creeping of the slope material may slowly deteriorate shear strength and create favorable conditions for slope failure. As mentioned prior, volcanic eruptions can also deposit material that overload a slope and cause it to fail.

Anthropogenic Factors

In addition to an array of natural processes that can result in slope failure, the role of human activity has become more important in recent decades. Extensive landuse and landcover changes in many parts of the world have severely altered the landscape. Large-scale development and industrial activities have imposed changes to landcover, climate, and hydrologic systems. Especially in mountainous regions, these alterations can have far-reaching implications for landslide susceptibility. Anthropogenic causes of landslides can be categorized into direct and indirect effects. The former includes human activities that directly impact some aspect of slope stability, including but not limited to, toe excavation, slope loading, drawdown, irrigation, and deforestation (Cruden & Varnes, 1996). The latter describes activities that indirectly create favorable conditions for slope failure. For instance, it is likely that increased greenhouse gas emissions, resulting from human activity, are shifting global climate patterns. These shifts influence the duration, and intensity of precipitation which in turn affects slope stability. Due to the complexity of the system, it is often difficult to identify the underlying dynamics that encourage favorable changes to landslide parameters.

For decades, anthropogenic activity has played a direct role in slope stability. During the construction of infrastructure, for instance, landscapes are fundamentally altered. Cruden and Varnes (1996) assert that toe excavation can, similar to toe erosion, remove necessary support that resists failure. Likewise, mining activities, or urban and industrial development in mountainous regions, frequently remove slope material to create more suitable building surfaces. During this process, necessary lateral support is removed at the toe of slope. If insufficient reinforcement measures are employed during construction, slopes are left highly susceptible to landsliding and exposed to the elements. Urbanization and the consequential expansion of impervious surfaces may also lead to higher peak floods and enhanced discharge that quickly erodes lateral support (Bonnard, Tacher, & Beniston, 2008). Additionally, in cases where fill material is carelessly deposited onto a slope, the added weight can overload weak parent material and result in failure. The mechanics are comparable to weight surcharges by glaciers, volcanic activity, or heavy precipitation (Varnes, 1978).

In addition to the structural changes presented thus far, road construction also changes natural hydrologic pathways (Sidle & Ochiai, 2006). Surface runoff is channeled in culverts and subsurface flow may be intercepted by impervious structures. Alteration of drainage dynamics for a hillslope may enhance its susceptibility to landslides, because a higher water table can result in meeting the saturation threshold much earlier. During rain events, poorly drained hillsides can take on less water before reaching complete saturation. Pore pressure may spike rapidly once full saturation has occurred. Generally, a decrease in intergranular pressure and friction can be observed (Varnes, 1978). In extreme cases, this liquification of the slope material may result in debris flows. Reaching the precipitation threshold can also result in surface runoff due to the soils inability to take on additional water. In these instances, rates of erosion are high and general stability is low (Varnes, 1984). It is important to note that the severity of these destabilizing factors depends heavily on design and construction standards (Sidle & Ochiai, 2006). Careful planning and proper geotechnical assessments can mitigate landslide risk. In view of staggering costs associated with this approach, however, crucial evaluations are often ignored.

Rapid surges in pore pressure, resulting from drawdown or excessive irrigation describe an additional anthropogenic cause for landslide activity. The effects of sudden changes in water level are naturally prominent along coastlines, rivers, and lakes (Wieczorek,

1996). During flooding events or extreme droughts, water levels can fluctuate substantially. Yet, drawdown effects can be artificially created through rapid dewatering. Especially near reservoirs, with frequently changing water levels due to dams and other obstructions, pore pressure changes in hillsides can be observed. When water level rises, pore pressure within the hillside increases which reduces effective strength of the slope material (Wieczorek, 1996). During drawdown, lateral support in banks along channels and reservoirs is removed (Varnes, 1984). The effects are similar to toe excavation during road construction. Increases in pore pressure are also observed after prolonged irrigation or pipe leakage (Sidle & Ochiai, 2006). Improperly designed storm drainages that divert water onto unstable areas can also result in saturation of slope material. The effects of human induced alterations of hydrologic properties are comparable to prolonged rainfall events that fully saturate hillsides. The addition of weight and the liquification of slope material contribute to general instability

Large-scale landcover changes can have a variety of impacts on the strength of slope material (Varnes, 1984). When considering the implications of deforestation for landslide susceptibility, it becomes apparent that by removing vegetation, several adverse conditions are created. First, bare hillsides absorb water faster which causes rapid increases in pore pressure to weaken the parent material. The additional weight imposed on the slope further intensifies stress. Second, without the additional cohesion strength of a dense root network, the soil mantle is more prone to landsliding (Sidle & Ochiai, 2006). Third, evapotransparitive properties of life vegetation help to regulate the water level within a slope. This ability is significantly impaired when extensive deforestation is occurring. Fourth, fluvial erosion, caused by altered runoff characteristics, may reduce toe strength and steepen an already stressed hillside. Subsequently, with enough water input from storm events or snowmelt, the probability of failure increases substantially. For that reason, it is essential to thoroughly analyze the impacts of various landslide causes and incorporate them in site development and construction activities.

Climate and Landslides in the Pacific Northwest

In the Pacific Northwest, hydrologic, vegetative, and geologic factors have been repeatedly linked to mass movement events (Swanston D. N., 1984). Along Oregon's coast,

landslide activity is prevalent in sedimentary rock and frequent during the rainy season which lasts from October to March (Schulz, Galloway, & Higgins, 2012). The combination of heavy precipitation, dependency on a vegetative cover, and weak geologic material can facilitate regional landslide risk. As outlined in the previous sections, the underlying causes of slope failure are well understood and extensively studied. However, the climatic factors that trigger landslides and the implications of climate change in the Pacific Northwest, find little acknowledgement in the scientific literature.

The Pacific Northwest receives the majority of its annual precipitation during the winter months (O'Connor, Hardison, & Costa, 2001). Intense storm systems deliver significant amounts of moisture between October and March. In higher elevations, precipitation is stored as snowpack. Due to extended periods of rainfall, many slope failures occur during the winter months. As outlined previously, the constant delivery of moisture may result in a complete saturation of the slope material. The additional weight of the water, as well as enhancements in pore pressure, can trigger mass movements. Similar processes can be observed during the spring, when melting snowpack causes overland flow and subsequent saturation of the slope material. Rapid surges in temperature during the spring also destabilize slopes by reducing soil cohesion provided by frozen water in the soil mantle. In addition, mild, humid conditions in coastal proximity encourage chemical weathering and result in a reduction of material strength among certain rock classes. The combination of topography and climate, make the Pacific Northwest highly susceptible to landslide activity. In view of rapid climatic changes, susceptibility will likely increase.

Currently used climate models suggest that the climate in the Northwest will warm over the next century. Historical climate records demonstrate that the Pacific Northwest warmed by approximately 0.6°C – 0.8°C since 1901 (Abatzoglou, Rupp, & Mote, 2014). Climate models predict that over the next century, warming trends between 0.1°C and 0.6°C per decade are possible in the Northwest (Mote & Salathe, 2010). Warming trends have serious effects on landslide potential in the Pacific Northwest for several reasons. First, increasing temperatures will alter snowpack and cause shifts in the timing of spring runoff (Clark, 2010). Thawing permafrost may destabilize slopes (Stoffel, Tiranti, & Huggel, 2014) and greater spring runoff may cause overland flow. In addition, earlier snowmelt runoff has been linked to increased wildfire occurrence throughout the western United States

(Westerling, Hidalgo, Cayan, & Swetnam, 2006). Because soil stability depends in large part on vegetation cover (Sidle & Ochiai, 2006), rises in wildfire frequency, corresponding to climate change, may increase landslide occurrence. Second, precipitation from extreme and heavy events is known to increase relative to more moderate events (Karl & Knight, 1998; Bonnard, Tacher, & Beniston, 2008). Model predictions indicate an increasing probability of intense future precipitation events in the United States (Groisman, et al., 2005), as well as increased spring precipitation in the Pacific Northwest (Miles, Snover, Hamlet, Callahan, & Fluharty, 2000). Since correlations between rainfall intensity and the occurrence of landslides are well established (Dhakal & Sidle, 2004), regional landslide susceptibility could expand significantly under future climate conditions. Especially shallow landslide potential is likely to increase in the 21st century, due to their vulnerability to prolonged, high-intensity storm events (Bonnard, Tacher, & Beniston, 2008). Complex modeling efforts are necessary to mitigate landslide risk, and protect valuable resources.

Modeling Approaches

There are many approaches to landslide hazard assessment. Two factors that distinguish the various approaches include data requirements and their utility at different scales. In its simplest form, landslide hazard analysis utilizes topographic, geologic, and landslide inventory data to conduct a qualitative assessment of a region. High risk areas are identified based on historic landslide events, geologic composition of the parent material, and slope and aspect parameters. Expert knowledge of the mechanics and the relationships between variables relating to slope failure is mandatory for producing useful hazard maps. The process can be extremely time consuming and statistical justification of the decision-making is challenging. A contrasting approach involves the statistical analysis of predictor variables for discovering underlying relationships within the data. By building sophisticated statistical models, landslide susceptibility can be evaluated at various scales. Data availability is the primary limiting factor for this approach. In addition, it requires a broad understanding of the processes being modeled and can be very computing intensive for regional evaluations of susceptibility. Turner and McGuffey (1996) propose a classification scheme that groups landslide hazard assessment approaches into four unique categories: landslide inventory,

heuristic approaches, statistical approaches, and deterministic approaches. There are additional classification schemes available that vary slightly in terms of grouping and terminology but, generally, they follow a similar pattern (Guzzetti, Carrara, Cardinali, & Reichenbach, 1999; Sidle & Ochiai, 2006). Most importantly, it is crucial to understand that the utility of each modeling approach is governed by the research objectives of individual studies. It is up to the researcher to decide on an approach that is most appropriate for the size of the study area and the goals of the analysis.

Aerial photography and field surveys can be helpful for creating landslide inventories and for mapping the spatial distribution of landslides. By calculating densities of known landslide locations, it is possible to gain a basic understanding of slope failure activities on a regional scale. Examples include an inventory of landslide deposits for San Mateo County, CA for computing densities and drawing isopleth maps (Wright, Campbell, & Nilsen, 1974). It allows for a quantitative comparison of landslide events in various parts of the county and gives decision-makers the opportunity to allocate resources for localized, in depth analyses. This approach assumes that future landslide events will likely occur in areas of previous failure. Several comparable methods have been proposed over the years (Campbell, 1973; DeGraff, 1985). The results can be very helpful for general regional planning purposes. However, although density calculations are fast, simple, and inexpensive, there are several limitations with this approach. Most importantly, terrain is quantified based on proximity to known or predicted landslide locations. This may become problematic in terms of prediction accuracy, because most environmental factors vary temporally and spatially. Distance based approaches do not account for the complexity of slope failure and are, for that reason, more appropriate for initial exploratory landslide analyses. They should be supplemented by more detailed models or localized, geotechnical evaluations.

Heuristic approaches incorporate geomorphologic expert knowledge in the mapping of landslides, and can be characterized as either geomorphic analysis or qualitative map combination (Turner & McGuffey, 1996). In both cases, a priori knowledge of all landslide causes and instability factors within a study region is necessary (Guzzetti, Carrara, Cardinali, & Reichenbach, 1999). Geomorphic analysis, a mostly qualitative approach, relies on the expertise of scientists to accurately assess the landslide hazard during field surveys (Turner & McGuffey, 1996). Decision rules for hazard assessment are, therefore, place specific and not

always entirely clear. As mentioned before, this denotes that quantification of decision rules and reproducibility of the research is difficult. Usually, outcomes (i.e. susceptibility classifications) cannot be applied to a new study area. To address this problem, a qualitative map combination approach can be used (Sarkar & Kanungo, 2004; Gorsevski, Jankowski, & Gessler, 2006). Instead of assessing landslide hazard in the field, expert knowledge is employed to assign weighting values to parameter maps (Turner & McGuffey, 1996). For example, after classifying site data into unique groups for slope, geology, landcover, and precipitation regimes, individual weights are assigned for each category and spatial unit (e.g. raster cells or polygons) based on knowledge of causal landslide factors. Weighting values are then summed for each spatial unit. Cells with large summation values correspond to high susceptibility, whereas units with lower counts are less likely to fail. This approach allows for a thorough analysis of the decision-making process, and makes it possible to replicate the results. The impacts of various parameters on hazard zonation are easily accessible to land managers. One of the drawbacks to this approach includes potential generalization. Furthermore, insufficient field data may lead to improper weighting of factors and misclassification of hazard zones (Turner & McGuffey, 1996).

Another popular approach to landslide modeling involves the use of statistics to establish hazard zones. In essence, statistical models rely on the assumption that the relationship between past landslides and instability factors allows inferences for future events (Guzzetti, Carrara, Cardinali, & Reichenbach, 1999). Statistics are used to determine the combination of casual factors that have resulted in previous slope failures to identify areas where similar conditions exist (Turner & McGuffey, 1996). Statistically based models can be either of bivariate (Soeters & Van Westen, 1996) or multivariate form (Baeza & Corominas, 2001; Carrara, 1983). Both methods have been successfully used to map hazard zones. Applicability of approaches should be determined on a case-by-case basis. Discriminant analysis (Carrara, et al., 1991), linear and logistic regression (Lee, Won, Jeon, Park, & Lee, 2015; Gorsevski, Gessler, Foltz, & Elliot, 2006), and neural networks (Ermini, Catani, & Casagli, 2005) are among the most popular methods currently used (Guzzetti, Carrara, Cardinali, & Reichenbach, 1999). Statistical landslide analysis examines instability factors for each mapping unit within a study region and compares it to the landslide presence or absence data for that respective unit. Mapping units can include grid-cells, terrain units, unique-

condition units, slope-units, and topographic units (Guzzetti, Carrara, Cardinali, & Reichenbach, 1999).

Finally, deterministic approaches have been extensively used to assess landslide susceptibility (Terlien, Van Westen, & Van Asch, 1995; Gökceoglu & Aksoy, 1996; Gorsevski, Gessler, Boll, Elliot, & Foltz, 2006). They require a relatively homogeneous distribution of geomorphic and geologic parameters, which makes them most appropriate for smaller areas (Sidle & Ochiai, 2006). None the less, the increasing availability of GIS technology has made deterministic modeling also applicable over larger studies areas, but substantial computing power is necessary to execute the models (Turner & McGuffey, 1996). Deterministic models utilize physical laws to calculate factors of safety (F_s). Depending on input parameters like pore pressure distribution or soil thickness, a factor of safety is calculated. Values significantly greater than 1 corresponds to stable slopes. As the factor of safety approaches 1, the hillside becomes increasingly unstable. If $F_s \leq 1$, theoretically, slope failure is inevitable. Even though it is an advantage to have quantitative values of stability, Turner and McGuffey (1996) caution that oversimplification among deterministic models can be problematic as well.

Research Questions

As outlined in this chapter, there is an array of modeling approaches available to landslide researchers. However, most traditional methodologies are designed for local susceptibility assessment only, and are not useful at regional scales. In addition, considerations about spatial non-stationarity in environmental data is often overlooked. Many environmental modeling inputs are spatially autocorrelated, and the impacts of individual predictors on landslide susceptibility vary across space. Without accounting for these spatial patterns, predictions may be inaccurate. For that reason, this study includes a regional, geographically weighted (GWR) logistic regression approach to landslide susceptibility analysis. Under some circumstances, GWR can significantly improve overall performance and accuracy of model predictions. Furthermore, GWR outputs offer a great level of detail that allow for better model calibration and mapping of individual coefficients across space.

Since GWR presents a relatively new modeling approach, academic landslide literature is limited on the topic. None the less, it is a technique that is gaining popularity in other fields and could significantly improve overall performance of susceptibility models. By considering spatial relationships, modeling results may improve in ways that can assist land managers in allocating limited financial resources and implement mitigation strategies at a regional scale. To determine the improvements possible with these approaches, and the insights they might provide into the underlying factors driving landslide susceptibility, the following research questions were pursued in this study:

1. For a large region in western Oregon, how well can a traditional logistic regression model predict regional landslide susceptibility?
2. Does the model performance improve with different modeling approaches, such as disaggregating the region into smaller areas, and using geographically weighted logistic regression?
3. Do the data and modeling approaches in this study provide insight into the role of geologic factors versus climatic factors in predicting landslide susceptibility?

CHAPTER 2: METHODODOLOGY

THE STUDY AREA

The study area encompasses a large portion of the State of Oregon, stretching from the Pacific coast to the Cascade Range. Data availability, the driving force behind this selection, resulted in a study area covering the following counties in their entirety: Benton, Clatsop, Columbia, Coos, Curry, Josephine, Lincoln, Polk, Tillamook, Washington, and Yamhill. The remaining counties located in the eastern part of the study area, including Clackamas, Douglas, Jackson, Lane, Linn, Marion, and Multnomah, are only partially covered in this study due to a lack of soils data. In view of the importance of soil parameters for landslide modeling, it was decided to exclude portions that are not part of the USDA/NRCS Gridded Soil Survey from this research. The geographic extent of the study area, therefore, stretches from approximately 125º W to 122º W and 46º N to 42º N.

Topography in the study area exhibits great variety, including a lower elevation coastal range that separates the shore from inland locations, the Klamath Mountains in the southwestern part of Oregon, the fertile, centrally located Willamette Valley that stretches from north to south across several counties, and the Cascade Range that bounds the study area to the east. Elevations range from sea level along the shore, to high alpine settings over 2000 meters in the east. The landscape is shaped by active plate tectonics and continued volcanic activity. Several volcanic peaks are located throughout the Cascade Mountains, most notably, Mount Hood (3425m), Mount Jefferson (3199m), the Three Sisters (southern peak 3157m), and Mount McLoughlin (2894m). Tectonic activity in the region is responsible for frequent earthquakes and volcanic eruptions which play an integral role in landslide dynamics. The presence of volcanic activity has created severe slope angles of more than 70 degrees in parts of the study area, resulting in slope instability concerns due to oversteepening.

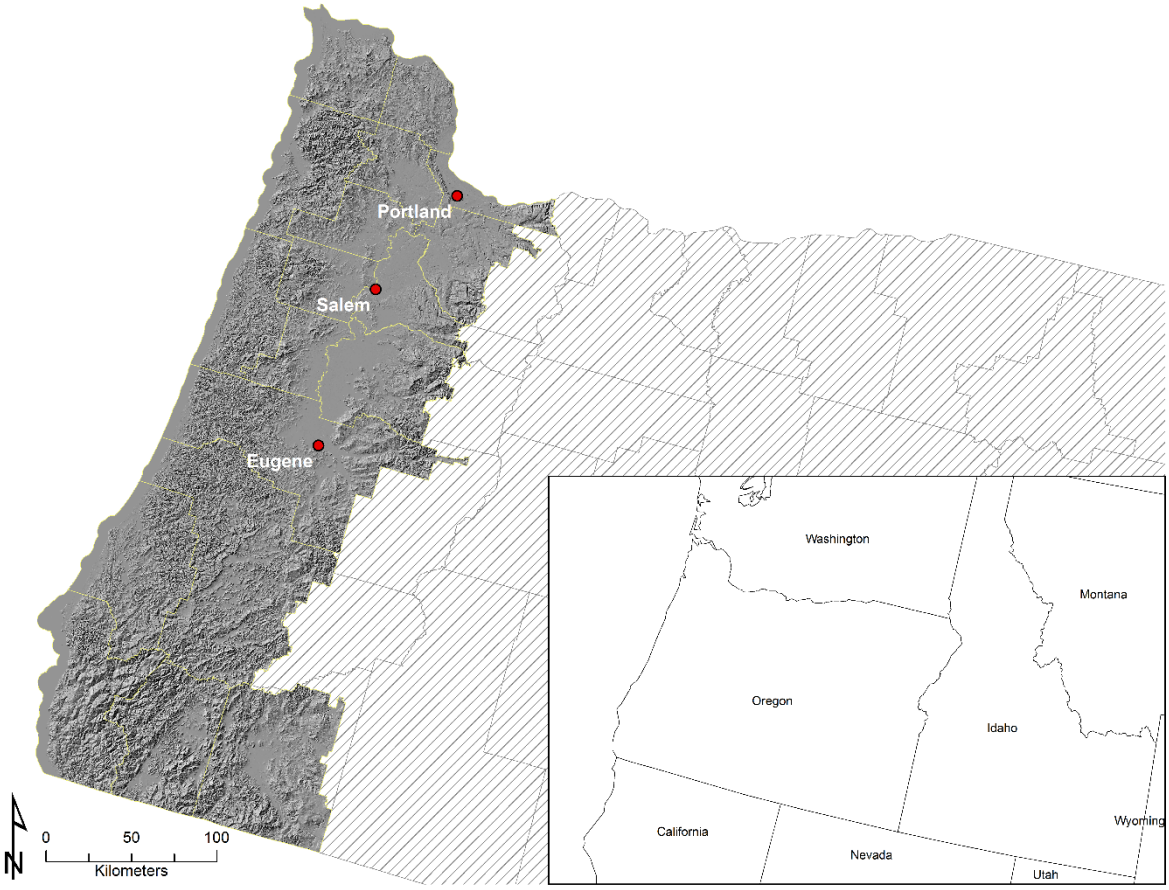

Figure 1. Overview of the Study Area

Geologic composition and soil parameters in the study area are also heavily influenced by volcanic activity. In the Cascade Range, the local geology is dominated by volcanic, volcaniclastic, igneous intrusive, and sedimentary rocks (O'Connor, Hardison, & Costa, 2001). Coastal regions are comprised of largely sedimentary and volcaniclastic rocks (Swanston D. N., 1984), while the Willamette Valley is dominated by sediments that originated from multiple Ice Age flooding events. The most prominent soil types in the study area include mollisols, generally associated with grassland ecosystems, inceptisols, often found on steep slopes in forested regions, and volcanic based soils, such as andisols, found in the northwestern part of the state.

The study area is situated in a temperate maritime climate with mild, wet winters and dry summers. In coastal proximity, temperatures depict little variability throughout the year. Mean annual temperatures reach approximately 12ºC in coastal regions. Further inland,

temperatures are a function of elevation with milder temperatures in the valley bottoms and colder conditions in alpine settings. Mean annual temperature varies between 11ºC in the lower elevations and 7ºC in higher elevations. Prevailing westerlies move air masses from the Pacific Ocean towards the Cascade Range where orographic lifting causes significant precipitation. Because of a northward expansion of the eastern Pacific high pressure system during the summer months, most precipitation falls between October 1st and May 31st (O'Connor, Hardison, & Costa, 2001). Precipitation increases with rising elevation, while temperatures decrease (Swanson & Swanston, 1977). An analysis of the west-east precipitation profile depicts 2000-3500mm of annual normal rainfall in the coastal range, 900-1200mm in the Willamette Valley, and 2500-3500mm on the western slopes of the Cascades. In higher elevations, winter storms form extensive snowpack that can last throughout the summer months.

Mountain ranges and higher elevation portions of the study area are generally covered by conifer forest. The timberline in the Cascades ranges from 2200-2500m (O'Connor, Hardison, & Costa, 2001) and forests consist of Douglas fir, western hemlock, and other coniferous tree species (Swanson & Swanston, 1977). In valley bottoms and lower elevations, shrub and herbaceous cover dominate the landscape. The fertile plain of the Willamette Valley allows for a variety of agricultural operations, and provides space for the three major population centers, Portland, Salem, and Eugene. Main transportation routes are confined to river valleys and lower elevations due to the challenging topography of the region.

Data Sources and Processing

Spatial datasets including landcover, elevation, geology, soils, climate, and historic landslide locations were obtained for the State of Oregon. Selection of appropriate environmental parameters was based on scientific literature and the physiographic setting of the study area. For the purpose of GIS-based modeling, spatial data was downloaded in raster format, or converted to raster cells with 30m spatial resolution. This allowed for a better transition between ArcGIS and other statistical software packages used in the study. One exception to this approach involved the acquisition of a landslide inventory. In this case, latitudes and longitudes for known landslide locations were downloaded to a geodatabase as

point feature. The reasoning for this decision was based on the study objectives which required a link between past climate conditions and landslide locations. Relevant geospatial layers, consisting of continuous and discrete variables, were imported into a preliminary geodatabase for further processing. The following paragraphs summarize data acquisition and function as a reference for future landslide susceptibility assessment in Oregon.

The fundamental element of this study is a statewide landslide inventory, SLIDO 3.2, published by Oregon's Department of Geology and Mineral Industries [DOGAMI]. The latest release is based on a project that commenced in 2007, intended to provide users with a base level of landslide data (Burns, Madin, & Ma, 2008). It offers a comprehensive, georeferenced collection of landslide research, totaling 12,095 historic events for release 3.2. The database is a compilation of a variety of published and unpublished studies for the State of Oregon. Newer releases included the addition of landslide deposits from Light Detection and Ranging (LiDAR), improvements to the database structure, and a procedure for continual updates (Burns & Watzig, 2014). SLIDO offers a comprehensive source of information for landslide research and contains crucial attributes like landslide type, date of failure, and slope angle, among others. The date component, listed for a significant number of records, permitted the modeling of past climate conditions utilized in this study.

The inventory includes landslide dates from the 1990s to 2014. However, due to the large variety of studies compiled in SLIDO, landslide data can vary greatly in terms of scale accuracy, and focus (Burns & Watzig, 2014). In addition, no efforts were made to verify the original data used in SLIDO (Burns & Watzig, 2014). Date components reflect the date of discovery and may not coincide with the actual failure date of the landslide. It is, therefore, necessary to emphasize that modeling outputs cannot replace site-specific geotechnical investigations. Instead, the results of this study should be used as a tool for regional planning and decision-making. After removing SLIDO records with missing date components, excluding failure events of the move class "rockfall", and eliminating slope movements outside of a 30m road buffer, a total of 1097 historic landslides were located within the study region. As mentioned earlier, data selection was driven by study objectives, focusing on road related landslides and their relationship with climate variables. Since rockfalls are generally associated with seismic activity, rather than precipitation and other hydrologic factors (Sidle & Ochiai, 2006), a decision was made to exclude such failure events from the analysis.

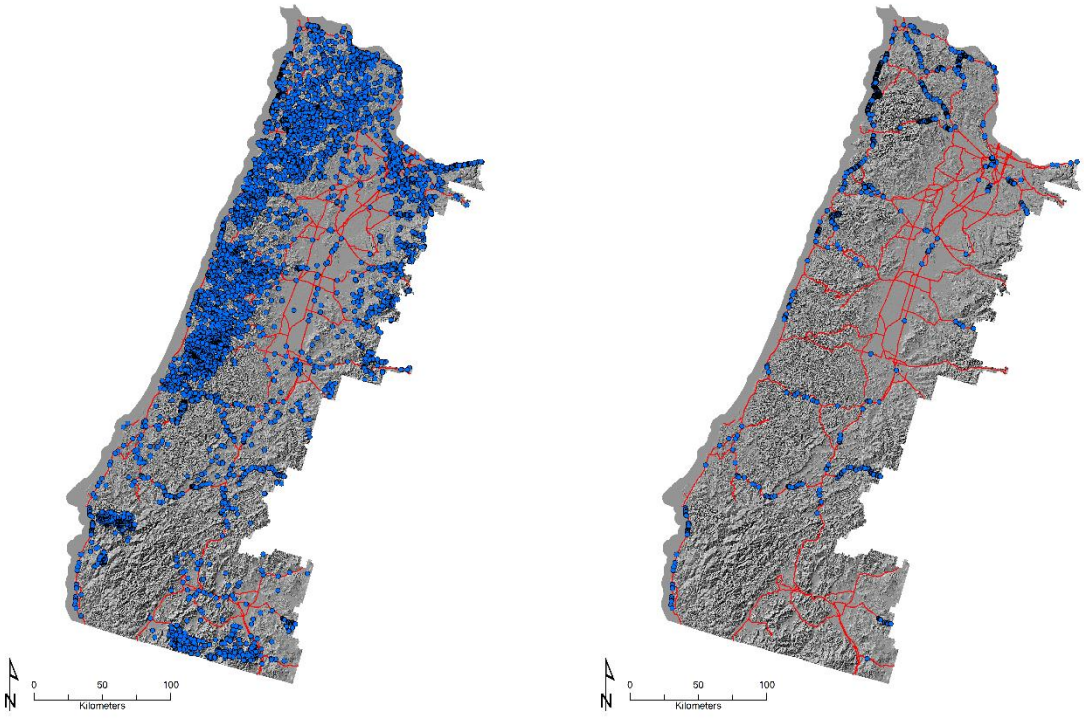

Figure 2. SLIDO 3.2 Historic Landslides vs. Modeling Inputs

Crucial physical landslide predictor variables, including slope, aspect, elevation, and curvature were derived from a 10m digital elevation model (DEM), acquired from the USGS (United States Geological Survey, 2016). Elevation products are made available as part of their 3D Elevation Program. The downloaded dataset provides continuous, statewide coverage of elevation parameters and complies with standard USGS data procedures. Geographic coordinates are in units of decimal degrees and elevation values are reported in meters. The DEM uses the North American Datum of 1983. Geospatial elevation data is useful for a variety of modeling applications, including hydrologic, resource, and habitat modeling. For this study, DEMs were utilized to compute slope, aspect, and curvature values across the State of Oregon. Additionally, planform and profile curvature were calculated for the study area. An elevation raster grid was created from the DEM, and all data layers were aggregated to 30m spatial resolution for alignment with other model inputs at coarser spatial resolution.

Table 2. Summary of Predictor Variables

Source	Parameter	Classes	Source	Parameter	Classes
SLIDO 3.2	Inventory	Landslide present	*gSSURGO*	Soils	Erosion Potential: Severe
		Landslide absent			Erosion Potential: Moderate
USGS DEM	Topography	Slope			Erosion Potential: Slight
		Aspect			Available Water Storage 0-150cm
		Elevation			Hydrologic Group A
		Curvuture			Hydrologic Class B
		Planform Curvutrure			Hydrologic Class C
		Profile Curvuture			Hydrologic Class D
LANDFIRE	Landcover	agricuklture	*METDATA*	Climate	Normal Annual Precipitation
		barren			Precipitation Anomaly Day of Landslide (DOL)
		developed			Precipitation Anomaly 1 day before landslide
		developed-upland			Precipitation Anomaly 2 days before landslide
		roads			Precipitation Anomaly 3 days before landslide
		shrub/herbaceous cover <50%			Precipitation Anomaly 4 days before landslide
		shrub/herbaceous cover >50%			Precipitation Anomaly 5 days before landslide
		snow			Precipitation Anomaly 6 days before landslide
		tree cover <50%			Precipitation Anomaly 7 days before landslide
		tree cover >50%			Cumulative Precipitation Anomaly 1 day before landslide
		water			Cumulative Precipitation Anomaly 2 days before landslide
OGDC-6	Geology	Volcaniclastic			Cumulative Precipitation Anomaly 3 days before landslide
		volcanic rocks			Cumulative Precipitation Anomaly 4 days before landslide
		vent and pyroclastic rocks			Cumulative Precipitation Anomaly 5 days before landslide
		terrestrial sedimentary rocks			Cumulative Precipitation Anomaly 6 days before landslide
		sediments			Cumulative Precipitation Anomaly 7 days before landslide
		metamorphic rocks			Absolute Precipitation Day of Landslide (DOL)
		melange rocks			Absolute Antecedent Precipitation 1 day before landslide
		marine volcanic rocks			Absolute Antecedent Precipitation 2 days before landslide
		marine sedimentary rocks			Absolute Antecedent Precipitation 3 days before landslide
		invasive extrsusive rocks			Absolute Antecedent Precipitation 4 days before landslide
		intrusive rocks			Absolute Antecedent Precipitation 5 days before landslide
gSSURGO	Soils	Alfisols			Absolute Antecedent Precipitation 6 days before landslide
		Andisols			Absolute Antecedent Precipitation 7 days before landslide
		Entisols			Normal Annual Temperature
		Histosols			Temperature Anomaly Day of Landslide (DOL)
		Inceptisols			Temperature Anomaly 1 day before landslide
		Mollisols			Temperature Anomaly 2 days before landslide
		Spodosols			Temperature Anomaly 3 days before landslide
		Ultisols			Temperature Anomaly 4 days before landslide
		Vertisols			Temperature Anomaly 5 days before landslide
					Temperature Anomaly 6 days before landslide
					Temperature Anomaly 7 days before landslide
					Temperature Day of Landslide (DOL)
					Antecedent Mean Temperature 4 days before landslide
					Antecedent Mean Temperature 7 days before landslide
					Antecedent Mean Temperature 14 days before landslide
					Antecedent Mean Temperature 28 days before landslide

Vegetation cover, an additional variable for comprehensive landslide analysis, was obtained from the LANDFIRE Project (United States Geological Survey, 2013). Their most recent product combines field survey data, satellite imagery, and statistical techniques to create a spatially explicit landcover dataset for the continental USA. LANDFIRE classifies existing landcover in 47 unique categories at a spatial resolution of 30 meters. Due to the

large extent of the study area, closely related landcover classes were collapsed into smaller groups to avoid the problem of separation during logistic modeling. The phenomenon of separation in models for binary responses arises when the covariates perfectly predict the dependent variable. Separation results in infinite coefficients and standard errors. By reclassifying the landcover data from 47 to 11 categories, problems related to separation are minimized. The final classification distinguishes between water, snow, agriculture, barren, developed, developed-upland, roads, tree cover >50%, tree cover <50%, shrub and herbaceous cover >50%, and shrub and herbaceous cover <50%.

Geologic data for landslide modeling was downloaded from Oregon's Geospatial Data Library. Release 6 of the Oregon Geologic Data Compilation, OGDC-6, was published by DOGAMI in 2015 and offers comprehensive, statewide geologic data (Smith & Roe, 2015). Like Oregon's landslide inventory, OGDC-6 is a compilation of a variety of published and unpublished studies with the purpose of making best known geologic mapping available to the public. The feature classes contained in OGDC-6 provide detailed information about fault lines, bedding, foliation, and other geologic parameters. For this study, general geologic rock types were used to describe the underlying parent material of the region. 11 unique geologic classes were extracted from OGDC-6 for modeling purposes. As other landslide research has demonstrated, the geologic composition can have far-reaching implications for overall slope stability (Sidle & Ochiai, 2006). In Oregon's Cascades and Coastal Range, for instance, a link between altered volcaniclastic rocks and slope failure has been observed (Swanston D. N., 1984).

Several important modeling components related to soils, were derived from the Gridded Soil Survey Geographic Database (gSSURGO), published by the United States Department of Agriculture. gSSURGO is an extension of the traditional soil survey product and formatted as file geodatabase (USDA/NRCS, 2014). The inclusion of 10-m raster data for soil units allows for high-resolution, statewide mapping of soil parameters. The highest level in soil taxonomy was chosen in this study to differentiate between soils. 9 out of 12 orders of soil taxonomy are distributed throughout the study region. They include alfisols, andisols, entisols, histosols, inceptisols, mollisols, spodosols, ultisols, and vertisols. Next, soil parameters related to erosion potential, hydrologic properties, and water storage capacity were obtained from gSSURGO for all map units in the study area. The hydrologic soil group

classification scheme provides valuable information about infiltration rates, runoff potential, texture, and soil composition throughout the soil horizon. They are important factors for landslide susceptibility and need to be considered for comprehensive modeling.

Finally, detailed meteorological data was downloaded for all landslide and non-landslide points based on location and date. The University of Idaho's Gridded Surface Meteorological Dataset (METDATA), was used to model past climate conditions. METDATA covers the contiguous United States with 4-km spatial resolution, and a temporal range from 1979 to 2016 (Abatzoglou, 2013). Daily precipitation and temperature values were extracted to compute 30-year normals, anomalies, cumulative anomalies, as well as antecedent rainfall and temperature conditions. These calculations were completed for 1097 landslide locations, and 22,997 non-landslide points. The temporal component for non-landslide points was established by analyzing the date range of landslide points and assigning a random date within that range. Since landslides used in this study occurred from 1996 to 2010, non-landslide dates cover the same timeframe. Modeling results could have been improved if the statistical distribution of landslide dates was considered during random date generation. Since, most random number generators utilize a uniform distribution, the underlying shape of the input data is disregarded. By matching the distribution of dates, more precise outputs could have been achieved.

METHODS

Data in this study was used to model the presence or absence of landslides along major roadways. The incorporation of climate variables was achieved by extracting historical precipitation and temperature values from METDATA. Other physical modeling inputs were assumed stationary. Except for landcover, latest releases of data products were utilized for modeling inputs. In the case of landcover, a 2011 product was selected because it most closely replicated the temporal range of the landslide inventory. Following the processing of environmental predictors in ArcGIS 10.3 and MATLAB, an exploratory data analysis was performed to discover underlying patterns and signals within the data. Subsequently, an exploratory regression in ArcGIS was used to evaluate all possible combinations of predictor variables. This step was important for recognizing issues of multicollinearity and spatial

autocorrelation. After defining a set of candidate explanatory variables, an ordinary least squares (OLS) model was fit. When no more improvements to the OLS model were possible, the raw data was imported into MATLAB for final logistic modeling and GWR4 for geographically weighted logistic regression (GWLR). Figure 3 outlines the modeling framework that was employed in this study.

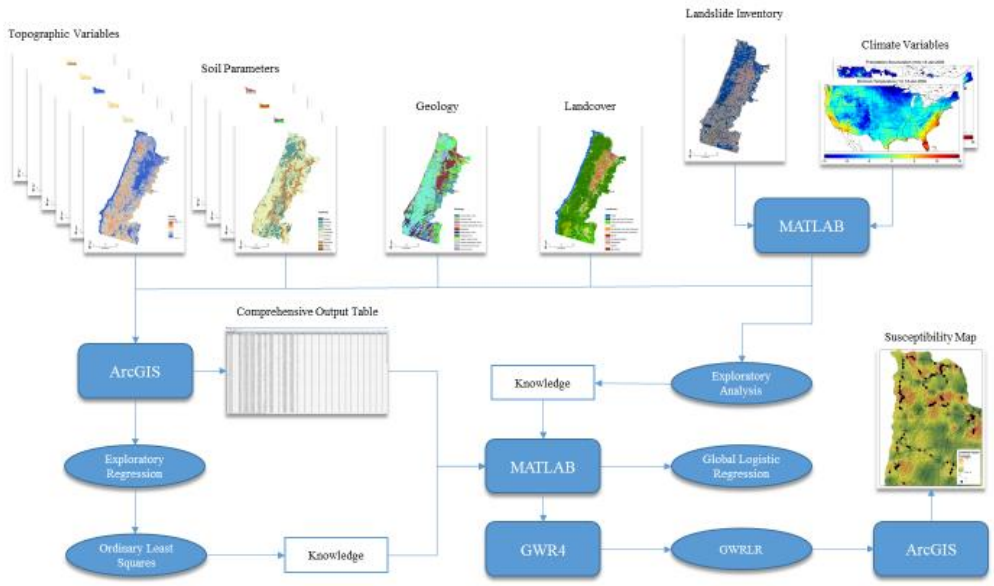

Figure 3. Flow-chart of Methodology

A grouping analysis was conducted in ArcGIS with all landslide/non-landslide point locations. By segmenting the inventory data into sub-regions, improved landslide predictions could be achieved. The subset of data was grouped based on the “mean annual temperature” attribute, because it allowed for the most appropriate segmentation of data points. By using temperature as the grouping variable, it was possible to create four groups with enough sample points to conduct a logistic regression analysis. During the grouping process, ArcGIS evaluates the optimal number of groups based on a Calinski-Harabasz pseudo F-statistic. By running the tool, the software is seeking to find natural clusters in the data. Groups are classified so that all features within a group are most similar, but groups themselves are significantly different from each other. Based on variable selection and nearest neighbor criteria, the grouping analysis classified four unique clusters for the study region. All

exploratory regression analysis was repeated for each sub-region. Global Logistic and GWR models were fit for all four groups, as well as the entire study region. Figure 4 displays the final segmentation of data points.

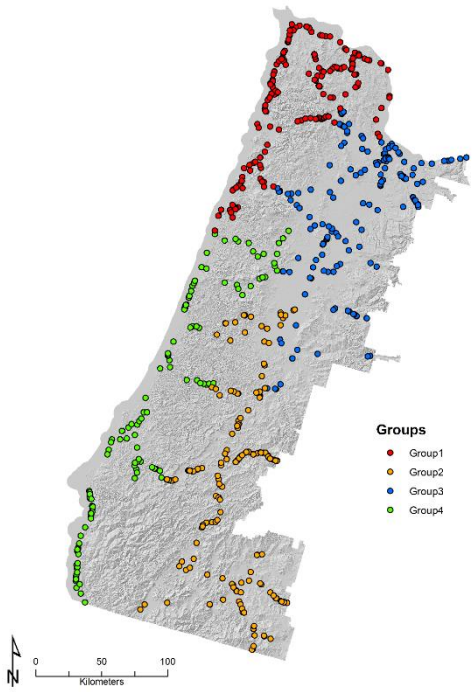

Figure 4. Normal Annual Temperature Segmentation of Data Points

Statistical Techniques

Logistic regression modeling in this study was completed in MATLAB. Like other statistical software packages, MATLAB allows for the fast and efficient processing of large datasets using a variety of analytical techniques. At its core, multivariate logistic regression analysis is appropriate for predicting the presence or absence of a phenomenon. A thorough discussion about assumptions, fit, and interpretation of logistic regression can be found in Hosmer et al. (2013). Logistic regression is among the most popular approaches for landslide modeling (Guzzetti, Carrara, Cardinali, & Reichenbach, 1999). Partly, this is the case because the method is very similar to standard linear regression, with the exception that the dependent variable, y, has a dichotomous outcome of either 1 or 0 (e.g. presence or absence of a landslide). By employing an appropriate link function, the logit, linear estimates between

positive and negative infinity can be transformed to probabilities between 0 and 1. From a set of continuous and discrete environmental variables, the model predicts the probability of landslide occurrence. An s-shaped curve is fitted to model the relationship between the dependent variable (y) and the predictor variables (x_n). The logistic regression model takes on the following form (Equation 1.1).

$$p(y = 1|x) = \frac{e^{\beta_0+\beta_1 x_n}}{1+e^{\beta_0+\beta_1 x_n}} \quad (1.1)$$

In this case, the probability of an outcome y=1 is computed by estimating values for the coefficients β_0, the intercept, and β_1, the slope of a predictor variable x_n. The least squares methodology that is often used in linear regression to estimate unknown parameters is not feasible for dichotomous outcomes (Hosmer, Lemeshow, & Sturdivant, 2013). Therefore, a maximum likelihood approach is employed to estimate β.

In its simplest form, a model consisting of only two predictor variables, slope and aspect, would take on the form outlined in Equation 1.2. For a set of predictor variables, the logistic regression model estimates the likelihood of landslide occurrence. One intercept and

$$p(y = 1|x) = \frac{e^{-6.93+0.09*SLOPE+0.43*ASPECT}}{1+e^{-6.93+0.09*SLOPE+0.43*ASPECT}} \quad (1.2)$$

one slope coefficient is estimated based on the regression inputs. In Equation 1.2, coefficients of 0.09 and 0.43, for the explanatory variables slope and aspect, indicate that landslide hazard increases as the values of these variables increase. If these coefficients were negative, this would denote that landslide hazard decreases as the values for slope and aspect increase.

None the less, by fitting one equation for all data points, a significant amount of spatial variability remains unaccounted for. Traditional logistic regression approaches do not consider the spatial dependence of environmental input parameters. To solve this problem, an extension to standard global logistic modeling is utilized in this study. Geographically Weighted Regression (GWR) incorporates local spatial relationships into a traditional regression framework (Fotheringham, Brunsdon, & Charlton, 2002). Mathematically,

Geographically Weighted Logistic Regression (GWLR), extends the standard equation for logistic regression (Equation 1.1.) with a spatial component (Equation 2.1).

$$p(y = 1|x) = \frac{e^{(\beta_0(u_i,v_i)+\beta_1(u_i,v_i)x_n)}}{1+e^{(\beta_0(u_i,v_i)+\beta_1(u_i,v_i)x_n)}} \quad (2.1)$$

The coordinate combination (u_i,v_i) is the location of a regression point i. For a model with 100 present and 100 absent cases, GWLR would evaluate a regression equation for 200 regression points. The selection of predictor variables remains static, but intercept and slope estimates are dynamic and dependent on location. This allows for an assessment of spatially varying regression coefficients.

In GWLR, local estimates are obtained by analyzing the neighborhood around regression points. A moving kernel evaluates data points based on their distance to the regression point and assigns weights (Fotheringham, Brunsdon, & Charlton, 2002). Closer data points are weighted heavier than points farther away. When data are sparse, a local model might be calibrated on very few data points when a fixed kernel size is selected (Fotheringham, Brunsdon, & Charlton, 2002). This could result in larger standard errors and is, therefore, undesirable. Since distances between data points varied significantly for the study area, fixed kernel sizes were inappropriate for local estimation of regression parameters. Instead, an adaptive Gaussian distribution was used in this study, because it is designed to adapt its size based on the data density (Fotheringham, Brunsdon, & Charlton, 2002). Consequently, in areas were data are sparse, kernels become larger and vice versa. The geographically weighted regression was carried out in GWR4. Optimal bandwidths for the adaptive kernels was evaluated based on Akaike Information Criterion (AIC) minimization.

CHAPTER 3: RESULTS

EXPLORATORY ANALYSIS

During the initial stages of modeling, the landslide inventory data was analyzed in MATLAB. Standard exploratory techniques were employed to study underlying processes in the data. Figure 5 illustrates the distribution of movement classes among the 1097 failure events. The high frequency of fill-failures results from resampling the original landslide inventory to satisfy study objectives. Fill-failures generally occur in regions of low relief, describing the failure of material associated with road-construction, mining, and other development (FEMA, 1989). Since it was the goal of this analysis to model the presence or absence of landslides along major roadways, many incidents involve the failure of fill material. The processes that trigger failures are identical to the landslide mechanics discussed in chapter 2. For all failure types identified in Figure 6, hydrologic factors play a significant role.

The distribution of landslides throughout the year is analyzed in Figures 7 through 11. For each sub region, as well as the global inventory, landslide dates were utilized to categorize failures by month. As mentioned before, this classification depends on the quality of the landslide inventory. Since no detailed field investigations were completed to verify these dates, it is possible that the month of failure coincides with the date of discovery rather than the actual date of failure. None the less, the histograms offer a good overview of the temporal distribution and help with the investigation of causal factors.

For the global inventory (Figure 7), incorporating groups 1 through 4, the largest number of landslides occurred during the months of August, May, and July, respectively. The large number of failure events during the summer months suggests that precipitation may not have been the driving forces behind these events, since July and August are usually the driest months of the year. An investigation of August landslides revealed that the majority of failures, 122 fill failures and 25 landslides, were recorded between 8/23/2010 and 8/26/2010 along state route 47 near Clatskanie, OR. It is possible that this distribution reflects a large-scale DOT effort to survey and record past landslide events, or that seismic activity had triggered several failures during that week. In summary, most frequent failures for groups 1,

2, 3, and 4, occurred in August, September, May, and February, respectively. While more events were reported during the summer months for groups 1, 2, and 3, most landslide events for group 4 occurred in the winter.

Winter landslides between November and March for the entire region totaled 296 events. From April to October, 801 events were registered. Figure 5 illustrates the distribution of summer and winter landslide, as well as a grouping of landslide events by year. It is noticeable that failure dates grouped by year appear clustered. For example, nearly all landslides in the southwestern part of the study region occurred in 2000 and numerous slope failures were reported in 2005 for the northern road segments of Highway 101. There are two likely explanations for these observed patterns. First, it is possible that government agencies received additional funding during those years and were mandated to locate and record historic failures in a particular region. However, only landslides with a particular date associated with them in the inventory were used in this analysis, suggesting that this is unlikely to be the main cause of this clustering. Generally, uncertainty regarding the date of failure was expressed in the inventory by simply leaving the date field blank or reporting just the year of failure instead of a specific date. In the SLIDO 3.2 landslide inventory, for instance, multiple records contain date attributes expressed as “1996?” or “1996-1997”. This suggests that the actual dates for these events weren’t entirely clear. Second, as mentioned previously, it is possible that special climatic conditions, such as prevalent storm tracks in years of particularly heavy precipitation, or other triggering mechanisms, such as volcanic eruptions or earthquakes, caused regional failures in certain parts of the study region. A local, statistical assessment of predictor variables is necessary to validate or refute such theories.

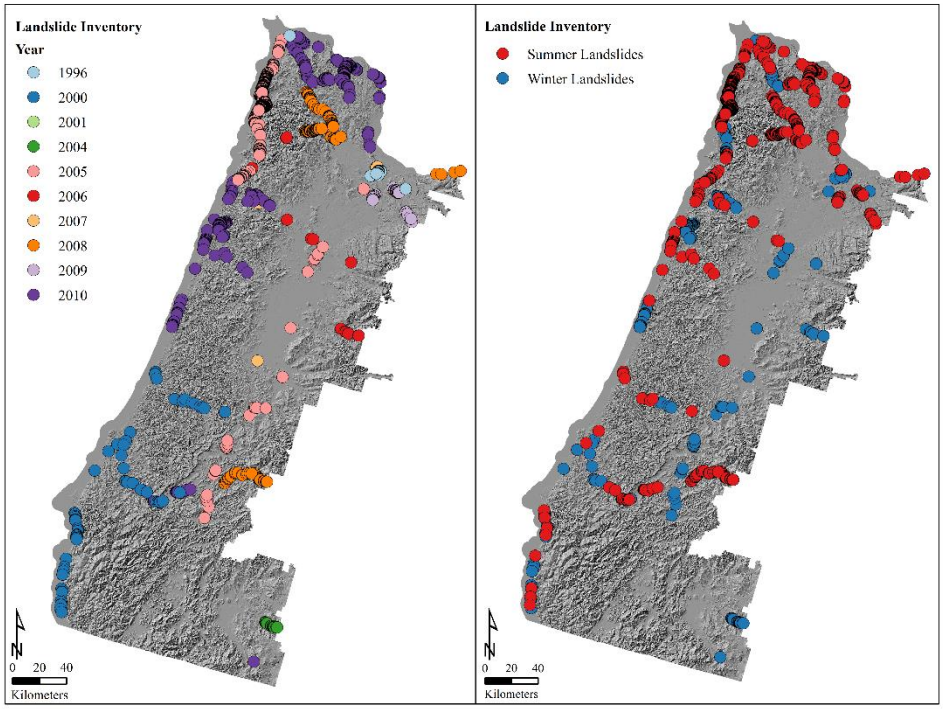

Figure 5. Yearly and Seasonal Distribution of Landslide Events

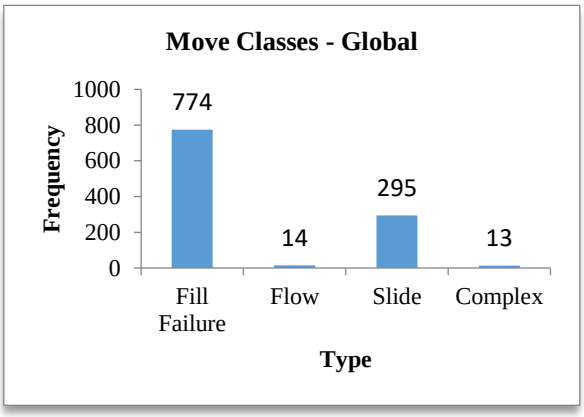

Figure 6. Move Classes of Landslide Inventory

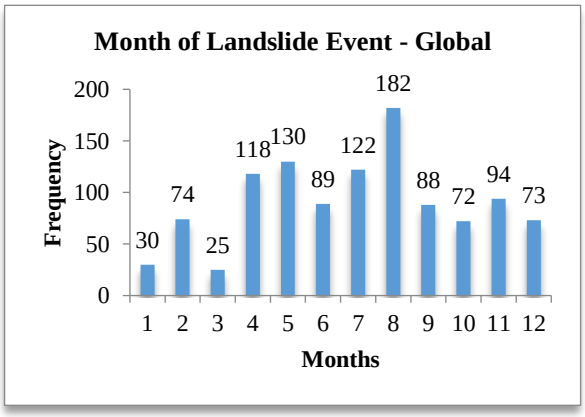

Figure 7. Distribution of Landslides (Global)

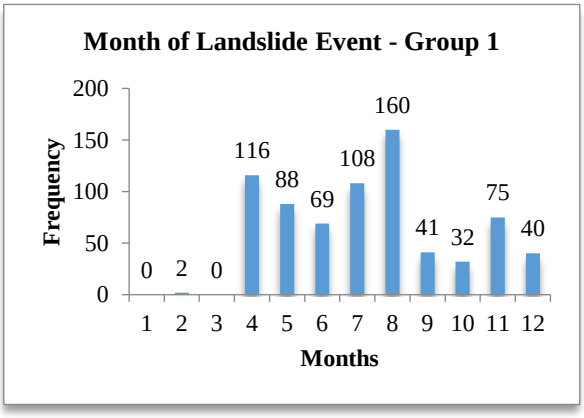

Figure 8. Distribution of Landslides (Group 1)

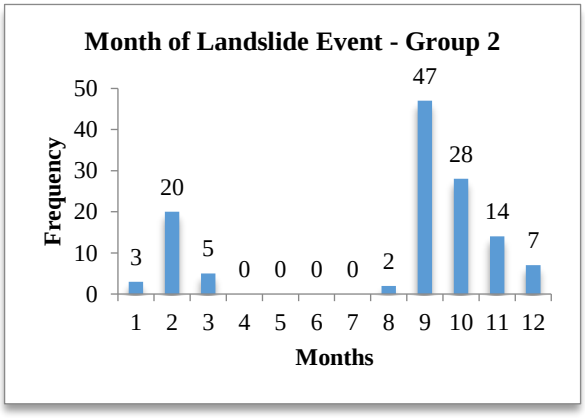

Figure 9. Distribution of Landslides (Group 2)

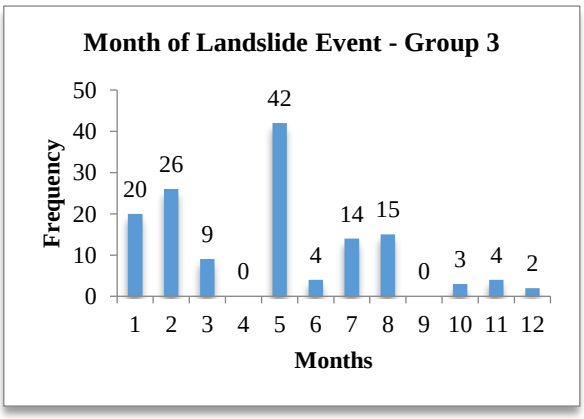

Figure 10. Distribution of Landslides (Group 3)

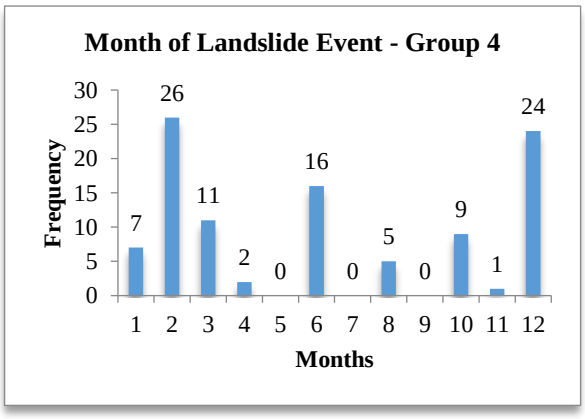

Figure 11. Distribution of Landslides (Group 4)

Long-term, gridded metrological observations were helpful for examining climatic conditions around the date of failure. By extracting relevant precipitation and temperature values based on latitude and longitude, composite graphs could be generated. Antecedent climate conditions for all sub regions are displayed in Figures 12 through 15. Composites are computed by averaging absolute, daily temperature and precipitation data across group samples. The resulting graphs showcase group specific climate conditions as a function of lead days before the reported slide. However, since group samples included landslides from 1996-2010, seasonality among groups is substantial. The graphs can help to explain some of the logistic regression parameter estimates, but can't replace event specific investigations.

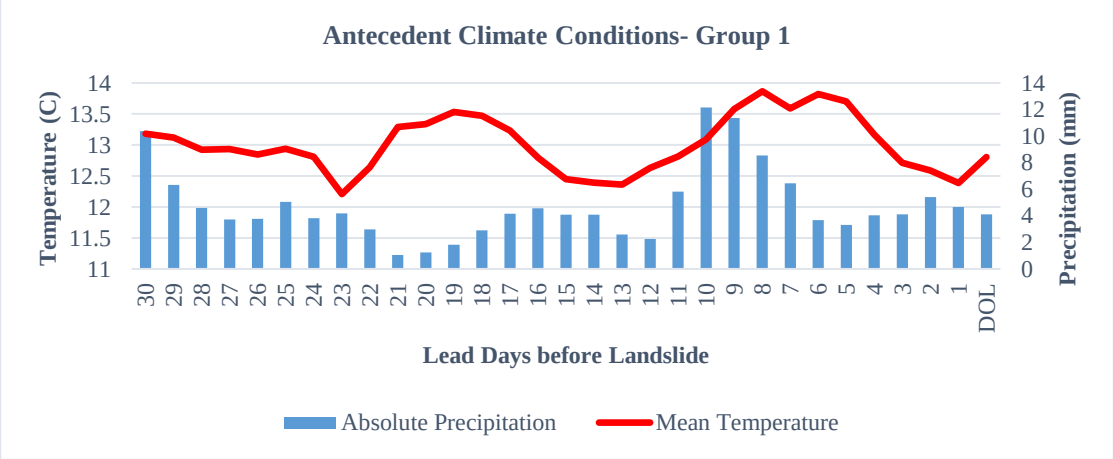

Figure 12. Antecedent T and PPT 30 Days Before Landslide Event (Group 1)

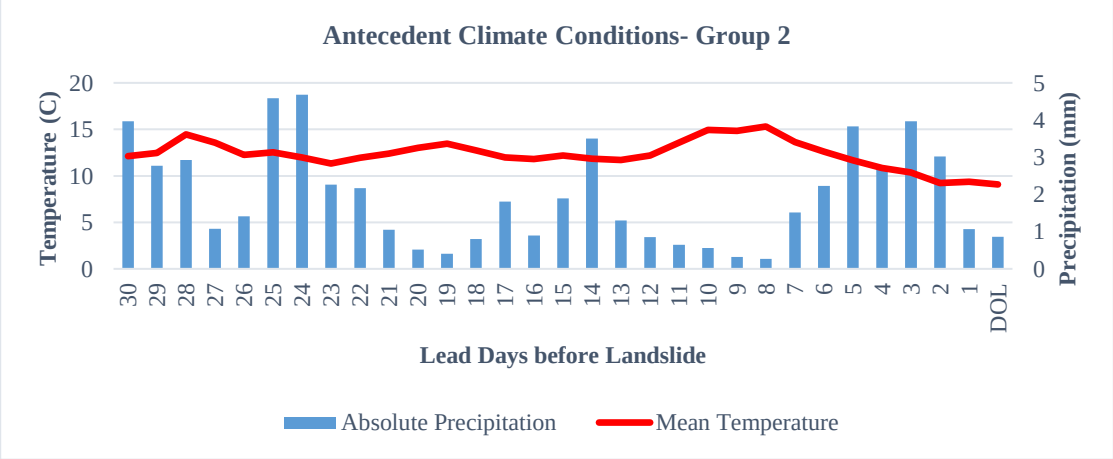

Figure 13. Antecedent T and PPT 30 Days Before Landslide Event (Group 2)

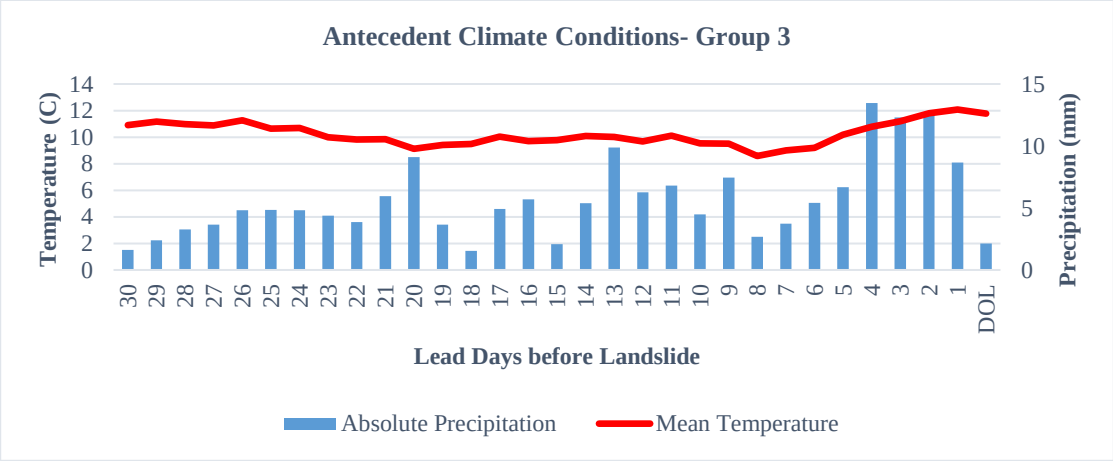

Figure 14. Antecedent T and PPT 30 Days Before Landslide Event (Group 3)

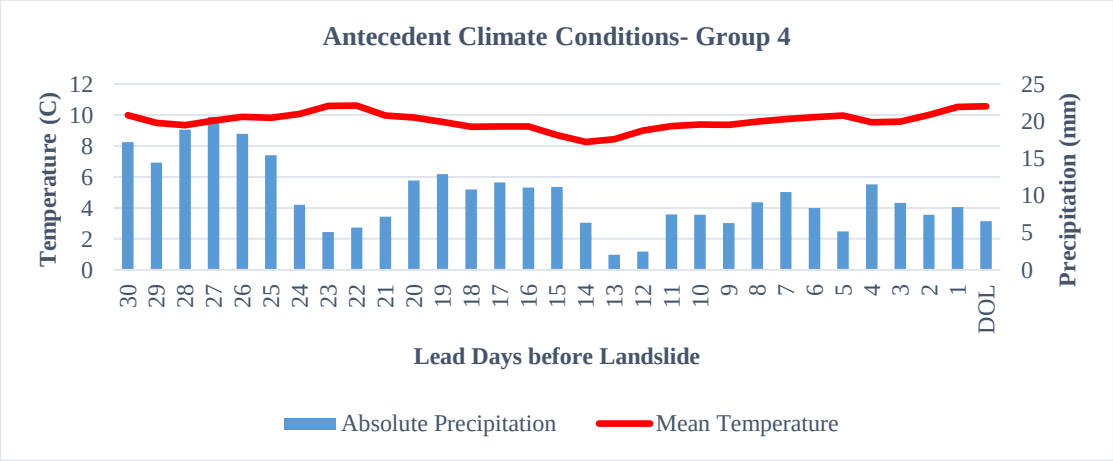

Figure 15. Antecedent T and PPT 30 Days Before Landslide Event (Group 4)

Slight increases in absolute precipitation 10 days before the landslide event is evident for all four groups. However, these surges are most likely not statistically significant. The magnitude of precipitation increase is especially distinct for sub regions 2 and 3, where rainfall amounts spike 3-4 days before the landslide event. In region 1, an increase in absolute precipitation can be observed 10 days prior to the failure. Mean daily temperatures fluctuate little in region 4, but are quite distinct for region 1. Overall, increasing trends in mean temperatures before the day of landslide can be observed in regions 3 and 4, approximately one week prior to failure. Decreasing trends are noticeable in region 2. For region 1, temperatures begin to decrease 7 days before the event, but then increase 1 day prior to failure. As mentioned before, group samples covered several years, and inter-annual

variability can certainly influence magnitude of the composite graphs. Without a uniform sample, bias from wet or dry years can potentially skew these composites. To account for some of the spatial variability in precipitation and temperature patterns, absolute values were compared to climate normals. Equations 3.1 and 3.2 were used to compute temperature and precipitation anomalies, respectively.

$$T_{anom} = T_{dailyMean} - T_{dailyClimatology} \tag{3.1}$$

$$PPT_{anom} = \frac{PPT_{daily}}{PPT_{dailyClimatology}} * 100 \tag{3.2}$$

Temperature anomalies are calculated by subtracting 30-year normals from the average daily temperature for a given day. Outputs reflect the temperature departure from normal in units of degrees. For precipitation, daily precipitation is divided by the 30-year normal precipitation for that day. This ratio is multiplied by 100 to obtain a percentage of normal. The following graphs, Figure 16 and 17, illustrate anomalies as a function of lead days before the reported slope failure.

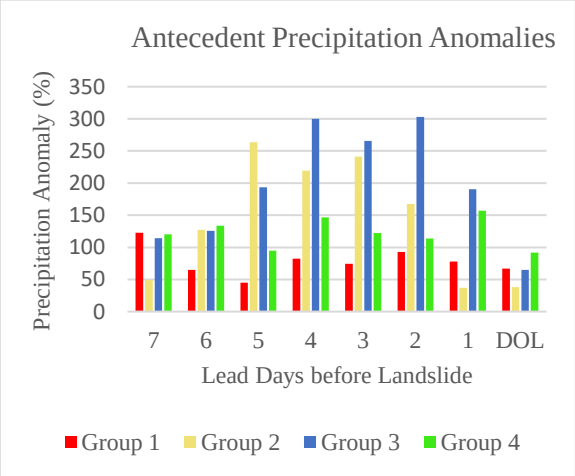

Figure 16. Antecedent T Anomalies

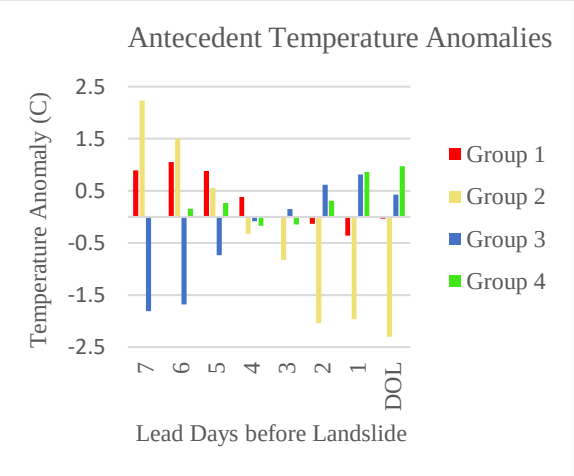

Figure 17. Antecedent PPT Anomalies

Some of the patterns that were previously observed for absolute values, are also evident when analyzing the anomalies. For regions 2 and 3, daily precipitation anomalies 2 to

5 days before the landslide are between 150% to 300% above normal. However, these spikes are not significant and should not be used for inferences about the data. Only one distinct signal could be identified when plotting composite anomalies for group 3 landslides between November and March (Figure 18). Precipitation anomalies increased to approximately 600% above normal 4 days before the landslide event. For the other sub regions, no clear weather drivers could be identified. In terms of temperatures, group 2 displayed a strong gradient of positive departures from normal of magnitude 2.2 ºC on day 7, to negative departures of 2.3 ºC on the day of landslide. For group 4, temperatures were generally warmer than normal before the failure date.

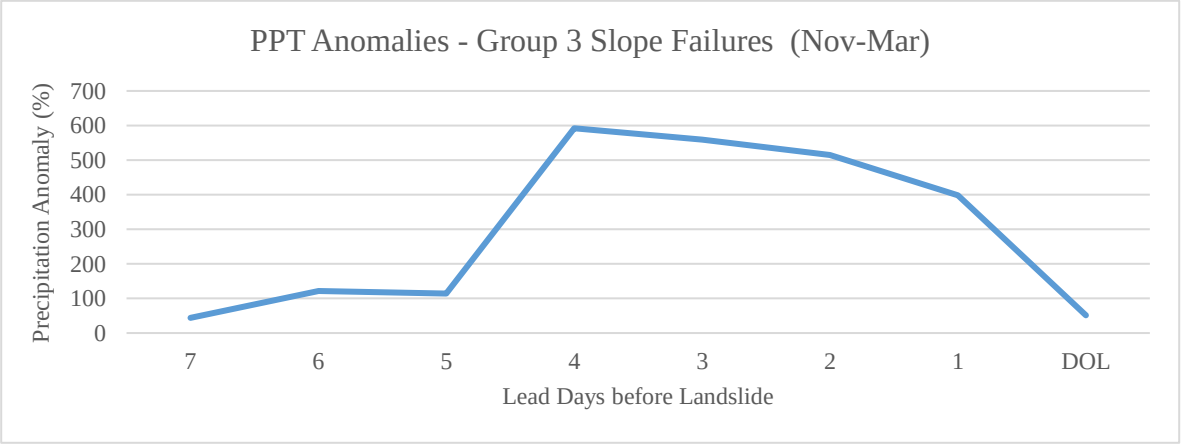

Figure 18. Precipitation Anomaly for Winter Landslides (Group 3)

Global Logistic Regression

Four logistic regression models were fitted for the sub regions, and one global model for the entire study area. Explanatory variables varied among regions, but certain predictors were included on a regular basis. Variable selection was driven by AIC minimization and considerations about coefficient significance. Table 3 illustrates the frequency of variable inclusion for 5 logistic models. Highly correlated predictor classes were combined for the purpose of calculating inclusion percentages. For example, a measure of erosion potential was included in all 5 models. However, while the “severe” erosion potential class was significant for groups 1, 2, and the global model, the erosion class “slight” was important for sub regions

3 and 4. The sign of the coefficients, as one might suspect, is positive for “severe” and “negative for “slight”. This denotes that landslide hazard increases as “severe” erosion potential increases, and that susceptibility decreases as “slight” erosion potential increases. Similarly, highly correlated geologic, hydrologic, and topographic classes were collapsed for Table 3. The results offer an overview of predictor importance for the study region.

The topographic variable slope was included in all models. This observation is consistent with results found in the common landslide literature. As slope angle increases, greater resisting forces are necessary for preventing failure. Depending on the composition of slope material and other environmental factors, stability can be significantly impaired on steeper hillsides. Additionally, hydrologic soil group classifications were frequently included in the logistic regressions. Hydrologic groups provide valuable information for landslide modeling, because their classification is based on soil composition. The distribution of sands, silts, and clays throughout the soil horizon allow for inferences about runoff potential, the rate of water transmission, and water holding capacity. Based on particle size, cohesion strength estimations can be attempted.

Table 3. Frequency of variable inclusion in LR models

Predictor	Global	Group 1	Group 2	Group 3	Group 4	% Inclusion
Erosion Potential	1	1	1	1	1	100
Hydrologic Soil Group	1	1	1	1	1	100
Slope	1	1	1	1	1	100
Geology_Volcanic	1	0	1	1	0	60
Aspect	1	1	0	0	1	60
Curvature	0	1	0	1	1	60
Vegetation Trees	1	1	0	1	0	60
3day Antecedent PPT	1	1	0	0	1	60
Day5_PPT Anomaly	1	0	1	0	0	40
DOL_PPT Anomaly	1	0	0	0	1	40
Day1_T Anomaly	1	1	0	0	0	40
Day2_T Anomaly	0	0	1	1	0	40
Day 7_T Anomaly	1	0	1	0	0	40
Andisols	1	1	0	0	0	40
Ultisols	0	0	1	1	0	40
Elevation	0	0	0	1	1	40
Geology_Sediments	0	1	0	1	0	40
Geology_Marine Sedimentary	1	0	0	0	1	40

Notes: Highly correlated predictor variables were combined

Other topographic variables, including aspect and curvature, were among the predictors in 3 of the 5 models. Aspect is commonly incorporated in landslide modeling because of its effects on local energy budgets and erosion rates. In the northern hemisphere, exposure to sun light is greater on southern slopes than on northward aspects. This can have a direct impact on vegetation density, and soil moisture, which are directly related to slope stability. Curvature was found among modeling parameters 60% of the time. It is often used in landslide susceptibility analysis because of its impact on hydrology. For example, in regions were planform curvature is concave, surface and groundwater channeling leads to increased activity of earth flows (Ohlmacher, 2007).

In terms of landcover, the vegetation class "trees" was included in the global model, as well as in sub regions 1 and 3. As mentioned in previous sections, root cohesion, erosion control, and pore pressure reduction through evapotranspirative processes are among the benefits of dense overstory vegetation. Indices for vegetation density, or landcover classes, are often used in landslide research because of their known correlation to slope stability. From the list of precipitation and temperature variables, 3 day antecedent precipitation was included in 3 of the 5 models. By summing absolute daily precipitation for the day of landslide and 3 preceding days, antecedent moisture is computed. Excessive delivery of precipitation causes several adverse effects including, liquification of slope material, fluctuations in groundwater flow, and weight surcharges.

Other climate variables, soil classes, and geologic parameters were included in 2 of the 5 models. Temperature anomalies for day 1, 2, and 7 before a landslide event, were found to improve model fit. During the winter months, rapid temperature fluctuations can enhance lateral pressure through frost action, or alter internal cohesion. Andisols, soil that is formed from volcanic ash, was a good predictor variable for the global model and region 1. This soil class is highly correlated with volcanic and volcaniclastic rock types. Sediments and marine sedimentary rocks were included in some logistic regression models. In Oregon's Coastal Range, deeply weathered siltstone and sandstone, the major lithologic constituents of marine sedimentary rocks, are often associated with creep and earthflow activity (Swanston D. N., 1984).

The results for the 5 logistic regressions models are displayed in Tables 4 through 8. Overall model fit improved when the dataset was segmented into regions. While the global

model only explained 23% of the deviance, regional models explained 36% to 75%. In addition, AIC scores were substantially lower for the regional models compared to the global model. The fitted model for region 2, demonstrated the best performance among the models. All but one explanatory variable, volcaniclastic geology, were significant at the 95% significance level. The model explained 75.3% of the deviance and had the lowest AIC score. Important predictor variables with positive coefficients included available water storage (AWS0150), slope, ultisols, severe erosion potential, hydrologic group D, precipitation anomaly 5 days before the landslide, and temperature anomaly on day 7. This denotes that landslide hazard increases as these variables increase. Negative coefficients for precipitation anomaly on day 7, cumulative precipitation anomaly 1 day before the landslide, temperature anomaly on day 2, and antecedent mean temperature for the 4 days preceding the landslide event suggest that landslide hazard decreases as these parameters increase.

The results for physical variables are consistent with the academic landslide literature. Slope generally exhibits a positive relationship, since steeper slopes increase the likelihood of landslide occurrence. Greater resisting forces are necessary to prevent hillsides with greater slope angles from failing. Similarly, with increasing water storage capacity, shear stress is enhanced due to the additional weight that is imposed on the slope once the soil becomes completely saturated. Soils with greater water storage capacity can retain more moisture which inadvertently leads to greater weight surcharges. The significant positive relationship between landslide hazard and severe erosion potential is also in agreement with other landslide research conducted. As a soils' k-factor, the factor of soil erodibility, increases, removal of lateral support during heavy rain or snowmelt events becomes more likely. Therefore, soils with larger k-factors, such as silts, have higher risks for lateral or underlying support removal. These soils are easily detached and produce high rates of runoff. Thus, increasing the landslide hazard substantially. The positive coefficient for hydrologic group D, is a result of the classification for this soil group. Group D soils have the greatest runoff potential and swell substantially due to their large clay content. When hydrated, clay rich soils expand and significantly increases lateral pressure. This process contributes to slope instability, and can also be observed in ultisols. As expected, the estimate for utilsols is positive. Thus, enhancing landslide hazard.

Interpretation of climate variables is more difficult, since only one clear weather driver for winter landslides in group 3 was identified during the exploratory analysis. None the less, the general distribution of anomalies shown in Figures 16 and 17, allows for some explanation of the sign of parameter estimates. In terms of temperatures, the logistic regression model for group 2 estimated positive coefficients for temperature anomaly on day 7, but negative coefficients for temperature anomaly on day 2, and antecedent mean temperature for the 4 days preceding the landslide. Composite temperature anomalies for group 2 showed that temperatures were 2.2 ºC above normal on day 7, but 2.0 ºC below normal on day 2. The parameter estimate on day 2 is negative, because landslide hazard decreases as below normal temperature approach normal. This is also the case for 4-day antecedent mean temperature. On the contrary, since composite temperatures were above normal on day 7, landslide hazard increases as temperatures depart above normal. In general, this suggests that above normal temperatures increase the landslide hazard.

For the precipitation estimates, explanation of the results is more challenging. The parameter estimate is positive for precipitation anomaly on day 5, but a negative on day 7. This is inconsistent with the landslide literature which suggests a positive relationship between precipitation anomalies and landslide hazard. The sign of the coefficients is most likely a remnant of two factors relating to data processing. First, by assigning dates to non-landslide locations based on a uniform distribution, inconsistencies among climate predictors may have been introduced. This denotes that the underlying distribution of landslides throughout the year was not considered. Second, since the landslide inventory covered events between 1996 and 2010, inter-annual variability among events is substantial. In order to better model the process of slope failure, it would be necessary to consider this variability during the exploratory analysis.

Table 4. Logistic Regression Results for Global Model

Variable	Estimate	SE	z(Est/SE)	Exp(Est)	Significance
Intercept	-2.068944	0.226485	-9.135012	0.126319	**
AspectCos	0.287005	0.157524	1.821977	1.332431	
Slope	0.108272	0.013662	7.925123	1.114351	**
Veg_TreeLe	-0.079366	0.313127	-0.253462	0.923702	
Andisols	-0.086238	0.303002	-0.284612	0.917376	
Mollisols	0.309022	0.236165	1.308499	1.362092	
Erosion_se	0.97272	0.21734	4.475571	2.645129	**
Marine_sed	0.167396	0.210212	0.796319	1.182223	
Volcanic	0.179022	0.300758	0.595236	1.196047	
Hydro_D	0.498957	0.222076	2.24679	1.647003	**
PPTanom_5day	0.111555	0.032753	3.405925	1.118016	**
PPTanom_DOL	-0.280624	0.071347	-3.933222	0.755313	**
PPTante_3day	0.020455	0.003474	5.888562	1.020666	**
TMEANanom_7day	0.07765	0.029323	2.648148	1.080745	**
TMEANanom_1day	-0.103927	0.034233	-3.035898	0.901291	**

Deviance:	800.75043	Classic AIC:	830.75043	AICc:	831.404381
Percent deviance explained:	0.229841	BIC/MDL:	900.051528		

Notes: ** - Significant at 0.05 level

Table 5. Logistic Regression Results for Group 1

Variable	Estimate	SE	z(Est/SE)	Exp(Est)	Significance
Intercept	-6.9306	1.462412	-4.739157	0.000977	**
AspectCos	0.429173	0.332896	1.289212	1.535987	
PlanformCu	-0.638643	0.54615	-1.169355	0.528009	
Slope	0.094223	0.028319	3.327151	1.098805	**
Veg_TreeLe	-0.681719	0.633525	-1.076073	0.505747	
Andisols	-0.398118	0.508978	-0.782192	0.671582	
Erosion_se	0.874368	0.472821	1.849258	2.397359	
Sediment	0.376443	0.455458	0.826516	1.457092	
Hydro_B	-0.066494	0.436236	-0.152428	0.935668	
PPT_AnnoNormal	0.000865	0.000458	1.889832	1.000866	
PPTcumanom_5day	-0.917947	0.41835	-2.194211	0.399338	**
PPTante_3day	0.048486	0.0144	3.367135	1.049681	**
TMEANanom_4day	0.318886	0.107659	2.962009	1.375594	**
TMEANanom_1day	-0.355113	0.106071	-3.347878	0.701094	**
TMEANante_28day	0.282353	0.05889	4.794549	1.326247	**

Deviance:	178.616997	Classic AIC:	208.616997	AICc:	211.225692
Percent deviance explained:	0.355775	BIC/MDL:	258.091757		

Notes: ** - Significant at 0.05 level

Table 6. Logistic Regression Results for Group 2

Variable	Estimate	SE	z(Est/SE)	Exp(Est)	Significance
Intercept	-4.03479	1.968465	-2.049714	0.017689	**
AWS0150	0.233255	0.084541	2.759065	1.262703	**
Slope	0.144803	0.050126	2.888777	1.155812	**
Ultisols	2.564067	1.160461	2.209525	12.988531	**
Erosion_se	3.472505	1.081043	3.21218	32.217353	**
Vol_clasti	-2.17992	1.127207	-1.933913	0.113051	
Hydro_D	3.417953	1.051934	3.249208	30.50689	**
PPTanom_7day	-1.675434	0.633318	-2.645484	0.187227	**
PPTanom_5day	0.486979	0.134857	3.611084	1.627393	**
PPTcumanom_1day	-2.481549	0.676588	-3.667739	0.083614	**
TMEANanom_7day	0.631215	0.1415	4.460883	1.879893	**
TMEANanom_2day	-0.820006	0.201159	-4.076409	0.440429	**
TMEANante_4day	-0.539581	0.126671	-4.259705	0.582993	**

Deviance:	68.36516	Classic AIC:	94.36516	AICc:	96.32215
Percent deviance explained:	0.753425	BIC/MDL:	137.243286		

Notes: ** - Significant at 0.05 level

Table 7. Logistic Regression Results for Group 3

Variable	Estimate	SE	z(Est/SE)	Exp(Est)	Significance
Intercept	10.230961	6.530723	1.566589	27749.17514	
Curvature	-0.084309	0.354156	-0.238057	0.919147	
Elevation	-0.010463	0.004542	-2.303878	0.989591	**
Slope	0.181732	0.045478	3.996035	1.199293	**
Veg_TreesM	-2.230947	1.163251	-1.917855	0.107427	
Mollisols	2.05861	0.651612	3.159258	7.835069	**
Ultisols	1.833474	0.744092	2.464041	6.25558	**
Erosion_sl	-1.459742	0.599128	-2.436443	0.232296	**
Vol_clasti	1.089021	0.940854	1.157481	2.971362	
Sediment	-0.275518	0.552716	-0.49848	0.759179	
Hydro_A	1.217375	1.220699	0.997277	3.378308	
PPT_DOL	-0.070475	0.040969	-1.720195	0.931951	
PPTante_5day	0.021457	0.006364	3.371514	1.021689	**
TMEAN_AnnoNormal	-0.995976	0.527006	-1.889876	0.369363	
TMEANanom_2day	0.139517	0.085801	1.62605	1.149718	
TMEANante_7day	-0.005681	0.041542	-0.136759	0.994335	

Deviance:	161.839506	Classic AIC:	193.839506	AICc:	196.812183
Percent deviance explained:	0.416287	BIC/MDL:	246.612583		

Notes: ** - Significant at 0.05 level

Table 8. Logistic Regression Results for Group 4

Variable	Estimate	SE	z(Est/SE)	Exp(Est)	Significance
Intercept	-0.638647	1.028223	-0.621118	0.528006	
AspectCos	1.113228	0.477405	2.331832	3.04417	**
Curvature	0.847601	0.390019	2.173229	2.33404	**
Elevation	-0.010198	0.004028	-2.531977	0.989854	**
Slope	0.130717	0.036635	3.568047	1.139645	**
Veg_Roads	1.590637	0.535823	2.968584	4.906872	**
Alfisols	2.319329	0.83936	2.763212	10.16885	**
Erosion_sl	-1.220315	0.659134	-1.851391	0.295137	
Marine_sed	0.264544	0.523252	0.505577	1.302837	
Volcanic	2.569393	1.675687	1.533337	13.0579	
Hydro_C	1.050883	0.543717	1.932777	2.860176	
PPTanom_DOL	-0.411469	0.161304	-2.550891	0.662676	**
PPTante_3day	0.014477	0.007811	1.853394	1.014583	
TMEANante_14day	-0.116614	0.074431	-1.566726	0.889929	

Deviance:	118.23726	Classic AIC:	146.237256	AICc:	149.348367
Percent deviance explained:	0.431399	BIC/MDL:	188.38615		

Notes: ** - Significant at 0.05 level

GEOGRAPHICALLY WEIGHTED LOGISTIC REGRESSION

Individual group data was imported in GWR4 where a geographically weighted logistic regression was performed. For each group and for the global case, the same independent variables were used for the GWR as were used during the logistic regression phase of the analysis. Therefore, the global model contained 15 exploratory variables, and groups 1, 2, 3, and 4 had 15, 13, 16, and 14 independent variables, respectively. A golden bandwidth search, utilizing AICc minimization, was selected for finding the optimal bandwidths for each of the 5 models. AICc is the Akaike information criterion corrected for a small sample bias. An adaptive Gaussian distribution was chosen to estimate varying coefficients across the study area. As mentioned previously, this type of function would reduce the effects of sparse data availability in parts of the study region, and worked best for this analysis. Tabular regression outputs for all models can be found in Tables 9 through 13. Individual parameter estimations are calculated for all regression points and vary across space. Therefore, result tables appear slightly different compared to traditional regression outputs. Mean, range, and other descriptive statistics are computed for individual explanatory variables to summarize the distribution of parameter estimates.

Regression diagnostics suggest that group model 2 provided the best fit for the data. The AIC of 70.5 for this sub region was substantially lower than scores computed for the other geographically weighted regression models. In addition, group model 2 explained 88.4% of the deviance, which is the highest percentage out of all models. Even though the optimal bandwidth for this group of 78.6 km was quite large, the results are still acceptable since data points for this sub region were more dispersed as shown in Figure 4. Group 1 had the lowest bandwidth of 55.2 km but only explained 55% of the deviance.

For geographically weighted regressions, cartographic visualization is an efficient way for displaying parameter estimates and associated levels of significance across space. Figures 19 through 23 show parameter estimates and pseudo t-values for the explanatory variable slope. This independent variable was selected for visualization purposes, because it was a significant contributor in all 5 regression models. For that reason, examination of varying parameter estimates across sub regions is possible. Map classification of coefficient estimates was based on a 5 class Natural Breaks grouping, available in ArcGIS. For t-values,

Table 9. GWLR Results for Global Model

	Estimate									
Variable	Mean	STD	Min	Max	Range	Lwr Quartile	Median	Upr Quartile	Interquartile R	Robust STD
Intercept	-2.220742	0.275027	-2.986973	-1.695606	1.291367	-2.362408	-2.231198	-2.072355	0.290053	0.215013
AspectCos	0.422868	0.233667	-0.045716	1.013789	1.059505	0.273064	0.365459	0.644521	0.371458	0.275358
Slope	0.113499	0.022551	0.05878	0.152447	0.093667	0.098229	0.117953	0.130899	0.032669	0.024217
Veg_TreeLe	-0.006352	0.279796	-0.493671	0.675642	1.169313	-0.250334	0.005259	0.195195	0.445529	0.330266
Andisols	-0.0548	0.600039	-0.874646	1.671702	2.546349	-0.51674	-0.291729	0.466812	0.983552	0.729097
Mollisols	0.446254	0.689362	-0.50843	1.634742	2.143172	-0.26389	0.466212	1.145985	1.409875	1.045126
Erosion_se	1.142606	0.333401	0.539019	1.672695	1.133677	0.824614	1.240835	1.400327	0.575713	0.42677
Marine_sed	0.277292	0.212411	-0.190496	0.806976	0.997472	0.150804	0.302626	0.368649	0.217845	0.161486
Volcanic	0.044305	0.326971	-0.711809	0.94123	1.653039	-0.171651	0.02843	0.224099	0.39575	0.293365
Hydro_D	0.604021	0.243781	0.125438	1.1067	0.981262	0.396169	0.625456	0.806137	0.409968	0.303905
PPTanom_5day	0.081679	0.10891	-0.224163	0.242796	0.466959	0.005165	0.086966	0.175261	0.170095	0.12609
PPTanom_DOL	-0.269318	0.074973	-0.411179	-0.130517	0.280662	-0.323598	-0.258747	-0.218579	0.105018	0.077849
PPTante_3day	0.017544	0.004393	0.005667	0.025098	0.019431	0.013673	0.018504	0.021355	0.007682	0.005694
TMEANanom_7day	0.09619	0.132916	-0.102889	0.345194	0.448083	-0.016896	0.060529	0.233975	0.25087	0.185967
TMEANanom_1day	-0.095767	0.072065	-0.210277	0.030727	0.241004	-0.164672	-0.092487	-0.024767	0.139904	0.10371

Deviance:	658.587222	AIC:	747.215362	AICc:	752.914499	
% deviance explained:	0.366573	BIC/MDL:	951.94961	Bandwidth:	159.493231	km

Notes: Robust STD is given by (interquartile range / 1.349)

Table 10. GWLR Results for Group 1

	Estimate									
Variable	Mean	STD	Min	Max	Range	Lwr Quartile	Median	Upr Quartile	Interquartile R	Robust STD
Intercept	-8.241576	2.017516	-11.774341	-5.53331	6.241031	-9.90937	-8.208953	-6.216639	3.692731	2.737384
AspectCos	0.652359	0.2567	0.222308	1.08841	0.866101	0.421844	0.743306	0.8509	0.429057	0.318055
PlanformCu	0.039525	1.073289	-1.917352	1.419043	3.336395	-0.621266	0.41895	0.900777	1.522043	1.128275
Slope	0.085622	0.017184	0.054364	0.116602	0.062237	0.071323	0.086695	0.095533	0.02421	0.017946
Veg_TreeLe	-0.599512	0.477719	-1.600953	0.067184	1.668137	-0.8773	-0.459402	-0.261941	0.615359	0.45616
Andisols	-0.208319	0.328496	-0.563435	0.62028	1.183715	-0.441691	-0.372642	-0.03919	0.402501	0.29837
Erosion_se	1.217292	0.282366	0.363789	1.752687	1.388898	1.072385	1.258602	1.432912	0.360527	0.267255
Sediment	0.391292	0.17499	-0.026619	0.675712	0.702331	0.303346	0.389083	0.540808	0.237463	0.176029
Hydro_B	-0.283207	0.290088	-0.833127	0.116755	0.949882	-0.503106	-0.253032	-0.026951	0.476155	0.352969
PPT_AnnoNormal	0.001035	0.000399	0.000279	0.001677	0.001398	0.000777	0.001118	0.001369	0.000593	0.000439
PPTcumanom_5day	-1.160746	0.899943	-3.185696	-0.254048	2.931648	-1.558183	-0.849873	-0.44588	1.112303	0.824539
PPTante_3day	0.058384	0.02757	0.02584	0.11675	0.09091	0.039304	0.045708	0.075929	0.036625	0.027149
TMEANanom_4day	0.439511	0.16161	0.15654	0.660287	0.503747	0.374356	0.490516	0.564087	0.189731	0.140646
TMEANanom_1day	-0.501272	0.234914	-0.899443	-0.128478	0.770964	-0.710408	-0.514674	-0.307137	0.403271	0.298941
TMEANante_28day	0.351281	0.118839	0.214852	0.594899	0.380047	0.241823	0.336313	0.441182	0.199359	0.147783

Deviance:	124.826076	AIC:	184.186197	AICc:	194.942001	
% deviance explained:	0.549785	BIC/MDL:	282.080456	Bandwidth:	55.166278	km

Notes: Robust STD is given by (interquartile range / 1.349)

Table 11. GWLR Results for Group 2

	Estimate									
Variable	Mean	STD	Min	Max	Range	Lwr Quartile	Median	Upr Quartile	Interquartile R	Robust STD
Intercept	-1.87242	3.271334	-6.843229	4.68508	11.52831	-5.514502	-1.227677	1.02551	6.540012	4.848045
AWS0150	0.225796	0.163779	-0.037968	0.535177	0.573145	0.084941	0.215092	0.389854	0.304913	0.226029
Slope	0.18558	0.08399	0.018155	0.318252	0.300097	0.16063	0.190023	0.254264	0.093634	0.06941
Ultisols	3.959437	1.349135	1.724711	6.508462	4.783751	2.98336	4.116588	4.99757	2.01421	1.493114
Erosion_se	3.860735	0.435854	3.268993	4.99067	1.721677	3.443378	3.905338	4.165789	0.72241	0.535515
Vol_clasti	-2.910826	1.794523	-6.03014	0.882621	6.912761	-4.258015	-3.558786	-1.925021	2.332994	1.729425
Hydro_D	4.261716	0.909517	2.961422	6.491871	3.530449	3.562541	4.277704	4.902036	1.339495	0.992954
PPTanom_7day	-2.169668	0.597915	-3.886805	-1.494144	2.392661	-2.599474	-2.062849	-1.684404	0.91507	0.678332
PPTanom_5day	0.618537	0.071186	0.466673	0.832058	0.365385	0.579727	0.629401	0.660017	0.08029	0.059519
PPTcumanom_1day	-3.771742	1.252874	-6.157772	-1.596969	4.560803	-4.829314	-3.825008	-3.136197	1.693117	1.25509
TMEANanom_7day	0.840135	0.252255	0.365657	1.248787	0.88313	0.766253	0.853784	1.043899	0.277646	0.205816
TMEANanom_2day	-1.177948	0.286204	-1.720497	-0.707801	1.012696	-1.41458	-1.185642	-1.021954	0.392626	0.29105
TMEANante_4day	-0.763548	0.183338	-1.166859	-0.444247	0.722612	-0.896117	-0.757055	-0.626982	0.269135	0.199507

Deviance:	32.22465	AIC:	70.532907	AICc:	74.825858	
% deviance explained:	0.883774	BIC/MDL:	133.709301	Bandwidth:	78.639493	km

Notes: Robust STD is given by (interquartile range / 1.349)

Table 12. GWLR Results for Group 3

	Estimate									
Variable	Mean	STD	Min	Max	Range	Lwr Quartile	Median	Upr Quartile	Interquartile R	Robust STD
Intercept	3.757066	9.038995	-10.322587	16.296004	26.618591	-6.235416	5.202041	12.612342	18.847758	13.971652
Curvature	0.21837	0.456679	-0.352018	1.47856	1.830578	-0.179587	0.182348	0.44744	0.627027	0.464809
Elevation	-0.012344	0.002348	-0.01913	-0.008737	0.010393	-0.013825	-0.011804	-0.010514	0.003311	0.002454
Slope	0.29892	0.103895	0.170113	0.533626	0.363513	0.204087	0.303049	0.395788	0.191701	0.142106
Veg_TreesM	-2.089403	2.127447	-6.462891	1.53015	7.993041	-3.762207	-1.845592	-0.119027	3.643179	2.700652
Mollisols	2.414814	0.799272	1.119359	3.913746	2.794387	1.824226	2.176416	3.262304	1.438078	1.066033
Ultisols	2.792148	1.075984	1.490538	4.641008	3.150471	1.59663	3.088747	3.93506	2.338431	1.733455
Erosion_sl	-1.392978	0.555843	-2.793752	-0.334533	2.459219	-1.7121	-1.500181	-1.006164	0.705936	0.523303
Vol_clasti	0.333871	0.566972	-0.877902	1.280127	2.158028	-0.053074	0.170137	0.846241	0.899316	0.666653
Sediment	0.383081	0.930569	-0.928337	1.973537	2.901874	-0.641305	0.711028	1.284209	1.925514	1.427364
Hydro_A	3.646132	2.510089	1.182972	9.016602	7.83363	1.392095	2.62542	6.029884	4.637788	3.437945
PPT_DOL	-0.024403	0.063405	-0.129676	0.075757	0.205433	-0.092278	-0.018971	0.040472	0.13275	0.098406
PPTante_5day	0.03078	0.012057	0.015927	0.052246	0.036319	0.017867	0.030453	0.043156	0.02529	0.018747
TMEAN_AnnoNormal	-0.639499	0.536552	-1.480783	0.291564	1.772347	-1.085415	-0.875708	-0.048875	1.036541	0.768377
TMEANanom_2day	0.182304	0.100284	-0.004228	0.519328	0.523556	0.121021	0.172321	0.201062	0.080041	0.059334
TMEANante_7day	0.046528	0.125525	-0.126115	0.29606	0.422174	-0.087197	0.039342	0.175327	0.262524	0.194606

Deviance:	94.72185	AIC:	153.481376	AICc:	164.005477	
% deviance explained:	0.658363	BIC/MDL:	250.385159	Bandwidth:	68.000000	km

Notes: Robust STD is given by (interquartile range / 1.349)

Table 13. GWLR Results for Group 4

	Estimate									
Variable	Mean	STD	Min	Max	Range	Lwr Quartile	Median	Upr Quartile	Interquartile R	Robust STD
Intercept	-0.676712	0.231484	-1.165786	-0.329252	0.836534	-0.851836	-0.687361	-0.465177	0.386659	0.286626
AspectCos	1.163647	0.420752	0.640674	1.726941	1.086268	0.743158	1.020906	1.564307	0.821149	0.608709
Curvature	0.782375	0.164332	0.554054	1.074864	0.520811	0.631001	0.733626	0.952866	0.321864	0.238595
Elevation	-0.012608	0.003906	-0.020742	-0.008834	0.011908	-0.015015	-0.011472	-0.009053	0.005962	0.00442
Slope	0.135086	0.0334	0.094701	0.200764	0.106062	0.107114	0.119439	0.164991	0.057877	0.042904
Veg_Roads	1.728733	0.452897	1.261355	2.563979	1.302624	1.329082	1.522867	2.173304	0.844222	0.625813
Alfisols	2.281058	0.350475	1.916122	2.744884	0.828763	1.940614	2.100376	2.698478	0.757864	0.561797
Erosion_sl	-1.163577	0.145692	-1.326401	-0.907563	0.418837	-1.300259	-1.215806	-0.987713	0.312546	0.231687
Marine_sed	0.467034	0.386795	-0.11935	1.021972	1.141322	-0.009296	0.557665	0.834435	0.84373	0.625449
Volcanic	3.234278	0.265984	2.799501	3.924894	1.125393	2.998323	3.233084	3.357551	0.359227	0.266292
Hydro_C	1.306299	0.094939	1.168193	1.492997	0.324804	1.217176	1.289911	1.387591	0.170415	0.126327
PPTanom_DOL	-0.37641	0.091321	-0.542205	-0.23546	0.306745	-0.478155	-0.343537	-0.317776	0.160378	0.118887
PPTante_3day	0.01877	0.015189	0.000976	0.045853	0.044877	0.00443	0.019954	0.030099	0.025668	0.019028
TMEANante_14day	-0.136773	0.021494	-0.177822	-0.115382	0.06244	-0.159203	-0.125444	-0.120247	0.038956	0.028877

Deviance:	94.284934	AIC:	137.583603	AICc:	145.284277	
% deviance explained:	0.546585	BIC/MDL:	202.761852	Bandwidth:	78.947204	km

Notes: Robust STD is given by (interquartile range / 1.349)

traditional cut points of 1.96 and 2.58, corresponding to the 95% and 99% significance levels, respectively, were selected (Fotheringham, Brunsdon, & Charlton, 2002). Parameter estimates for slope were positive in all 5 models, suggesting that landslide hazard increases as slope increases. The 5-class grouping of parameter estimates in Figures 19 through 23 shows how estimated coefficients change across space.

For the global model (Figure 19), modeling results suggest that parameter estimates for the variable slope vary substantially across the study area. While lower estimates tend to cluster in the northwest and the central part of the study region, higher values are found in the southern part. This sort of detail, which is very important for the interpretation of results, is lost when a standard logistic regression approach with one single global average parameter estimate is used. Most estimates are significant at the 99% level. When examining the t-values for region 1 and 2, on the contrary, it becomes clear that significance of parameter estimates also varies across space. For region 1, many parameter estimates are not significant at the 95% level in the northwestern part, but highly significant in the south. Subsequently, in region 2, a north-south trend is evident. Estimates become more significant as we move south across sub region 2. This is an interesting discovery since the global logistic regression model suggested that the variable slope was significant for all sub regions.

An Inverse Distance Weighting (IDW) interpolation was computed for GWR model predictions, to visualize landslide susceptibility across the study region. Major roads were buffered to limit the interpolation. Since all landslide events used in this analysis were located along roads, interpolation outputs with increasing distance from roads become less accurate. Subsequently, these areas were excluded from the final map product. A more spatially uniform landslide inventory would be necessary for creating a continuous prediction surface. Without it, predictions in remote areas have little statistical significance. The results of the IDW interpolation are displayed in Figure 24. Areas of low landslide susceptibility include the Willamette Valley, where little topographic variability is evident, and the southeastern part of the study area. Higher probability of landslide occurrence was computed for the Portland urban area and several road segments along Highway 101 and State Route 42. Along the coast, easily weathered sedimentary rocks and porous volcanic formations contribute to the landslide hazard. In addition, steep, west facing slopes influence susceptibility in these areas.

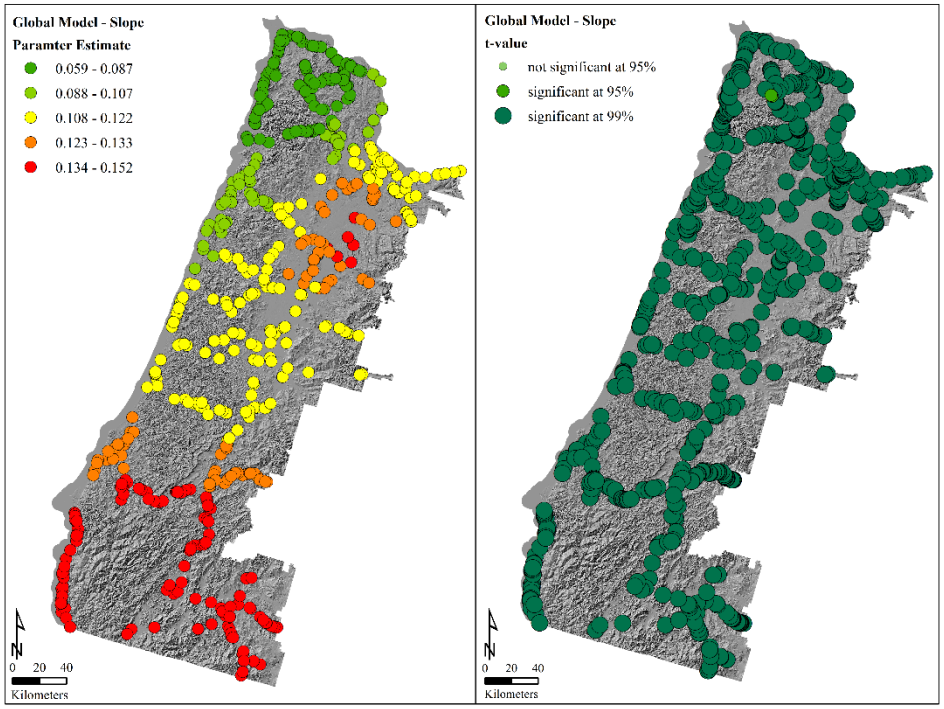

Figure 19. GWLR Estimate and Significance of Slope Variable (Global Model)

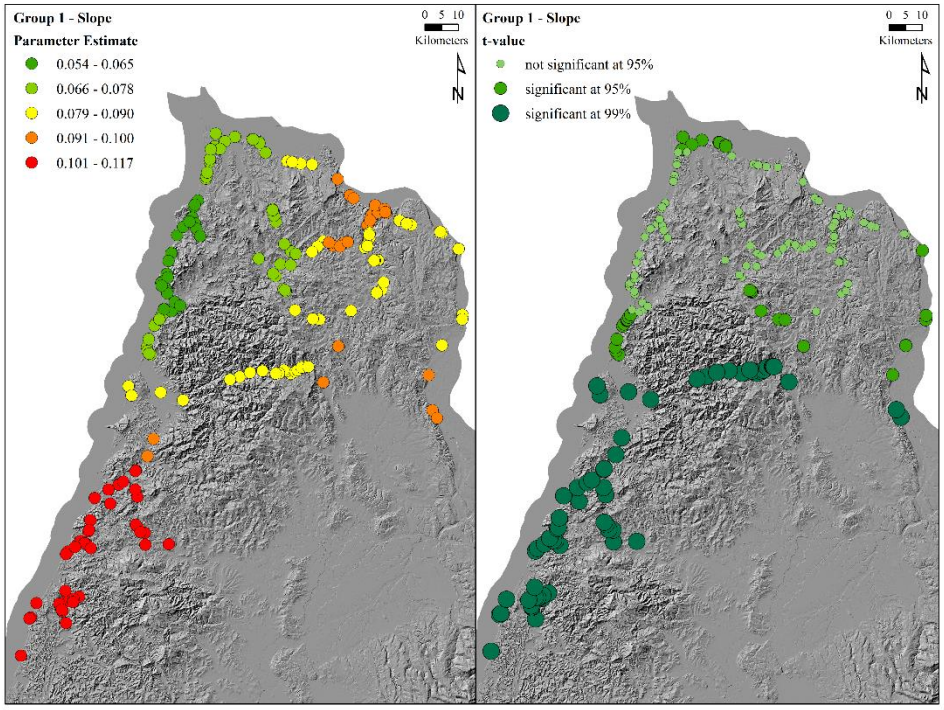

Figure 20. GWLR Estimate and Significance of Slope Variable (Group 1)

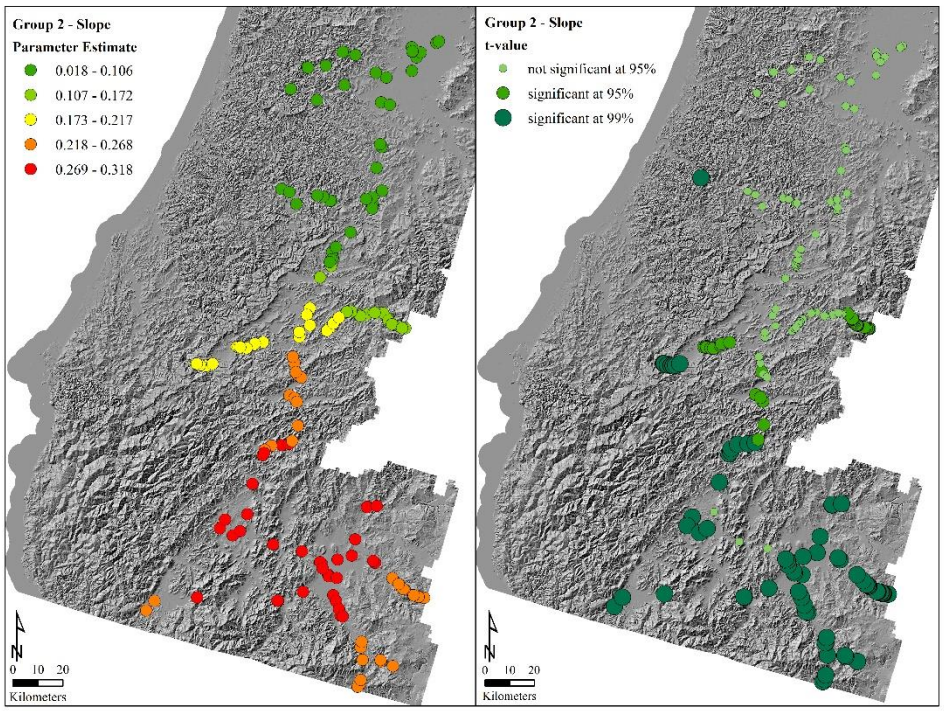

Figure 21. GWLR Estimate and Significance of Slope Variable (Group 2)

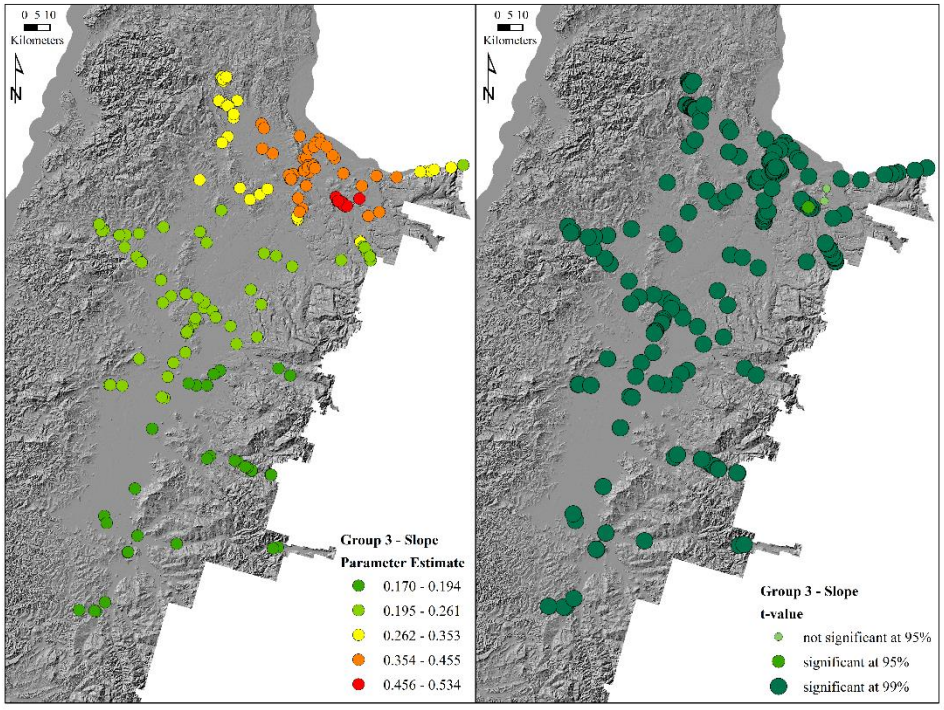

Figure 22. GWLR Estimate and Significance of Slope Variable (Group 3)

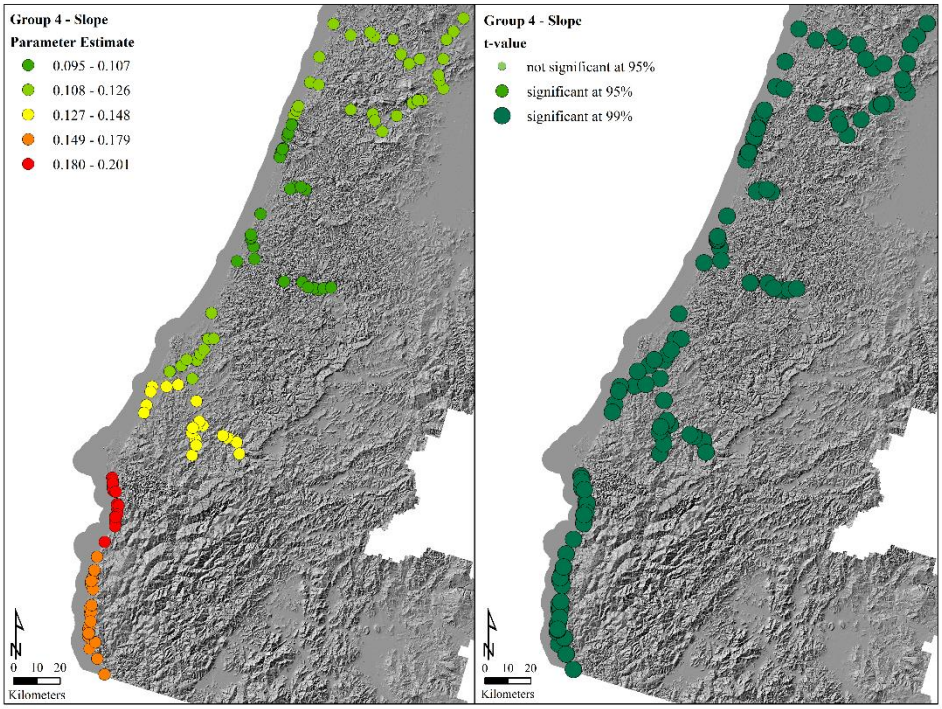

Figure 23. GWLR Estimate and Significance of Slope Variable (Group 4)

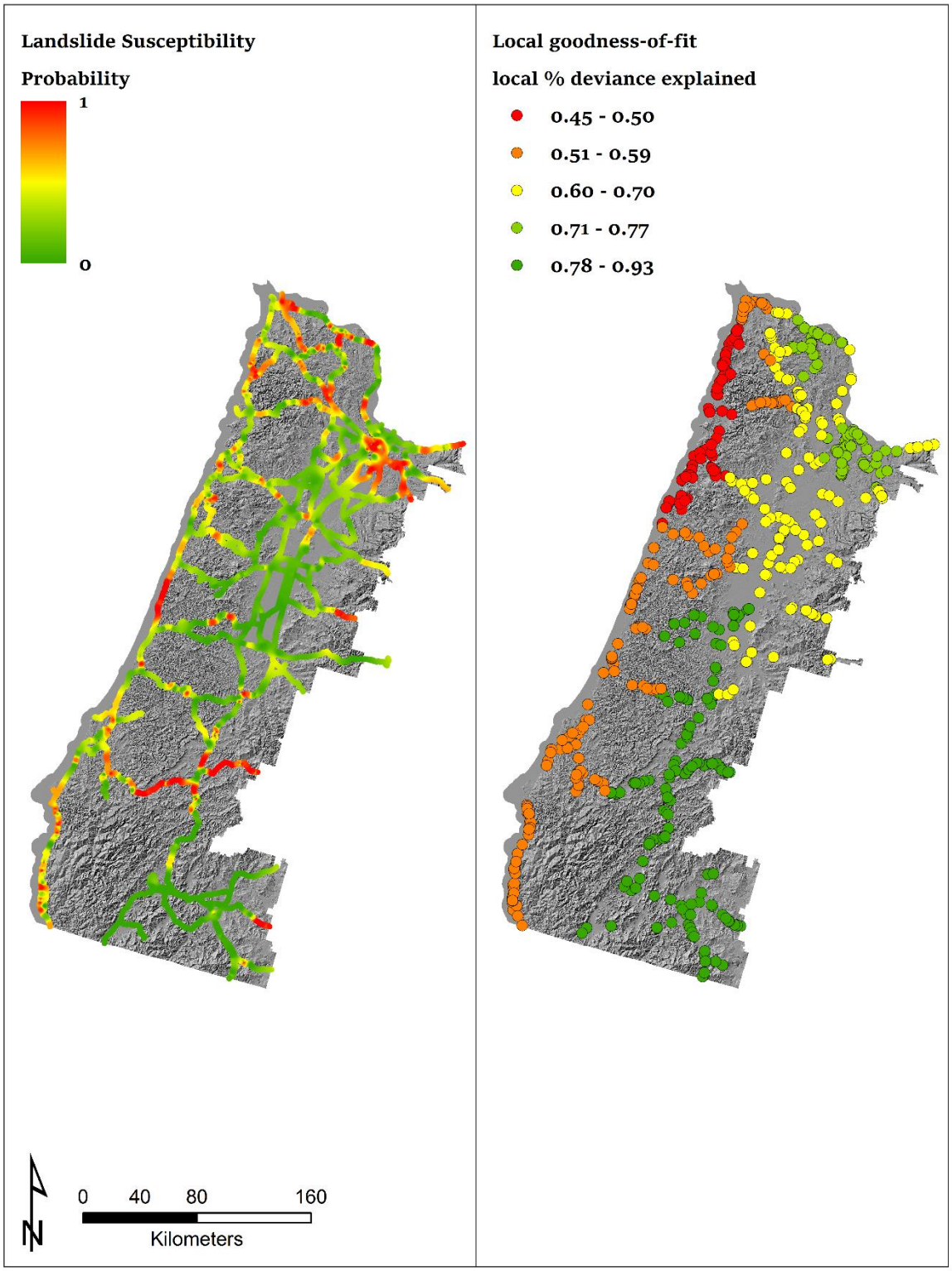

Figure 24. Interpolated GWR Predictions

MODEL COMPARISON

When analyzing the outputs from the traditional logistic regression and the geographically weighted logistic regression models, it becomes clear that the GWLR models outperformed standard techniques across all sub regions. Overall fit improves significantly when applying a GWLR. This suggests that GWLR predictions are more accurate. In addition, since GWLR also accounts for some of the spatial non-stationarity, results are more reliable across the study region. As outlined in the previous sections, AIC scores are consistently lower and GWLR models explain more of the deviance. Table 14 summarizes model diagnostics for the two approaches.

Table 14. GWLR - LR Model Comparison

	AIC		% deviance explained	
	LR	GWLR	LR	GWLR
Global	830.750	747.215	0.230	0.367
Group 1	208.617	184.186	0.356	0.550
Group 2	94.365	70.533	0.753	0.884
Group 3	193.840	153.481	0.416	0.658
Group 4	146.237	137.584	0.431	0.547

For the global model, AIC improvements were most significant. An improvement of more than 83 points suggests that the GWLR model provides a much better fit to the data. Since both models were trained with the same selection of landslide and non-landslide points, it can be concluded that GWLR presents a more practical approach for the data used in this study. On average, applying a geographically weighted regression lowered AIC scores by 36 points. Across all sub regions, GWLR models explained more of the deviance than standard logistic regression models. For region 4, the GWLR explained 65.8 percent of the deviance which is an improvement of more than 24% compared to the traditional approach. On average, GWLR explained 16% more deviance than LR models.

In terms of accuracy, GWLR model predictions were better across all regions. Classification tables 15.1 through 19.2 compare correctly and incorrectly identified landslide

events for each model. A traditional cutpoint of p=0.5 was used to distinguish between present and absent cases. Sensitivity, the proportion of correctly identified landslides, and specificity the proportion of correctly identified non-landslide points were computed for each model. In addition, overall model accuracy was calculated. Greatest improvements could be observed for region 1, where accuracy improved by 9.5% when moving from a standard logistic regression model to a geographically weighted logistic regression approach.

Table 15.1 Classification Table Based on Global LR

		Observed		Total
	Predicted	0	1	
	0	276	99	375
	1	98	277	375
	Total	374	376	750
Sensitivity	**73.7%**	Specificity	**73.8%**	Accuracy	**73.7%**

Notes: Cutpoint of p=0.5 was selected for classification

Table 15.2 Classification Table Based on Global GWLR

		Observed		Total
	Predicted	0	1	
	0	295	80	375
	1	60	315	375
	Total	355	395	750
Sensitivity	**79.7%**	Specificity	**83.1%**	Accuracy	**81.3%**

Notes: Cutpoint of p=0.5 was selected for classification

Table 16.1 Classification Table Based on Group 1 LR

		Observed		Total
	Predicted	0	1	
	0	80	20	100
	1	26	74	100
	Total	106	94	200
Sensitivity	**78.7%**	Specificity	**75.5%**	Accuracy	**77.0%**

Notes: Cutpoint of p=0.5 was selected for classification

Table 16.2 Classification Table Based on Group 1 GWLR

		Observed		Total
	Predicted	0	1	
	0	86	14	100
	1	13	87	100
	Total	99	101	200
Sensitivity	**86.1%**	Specificity	**86.9%**	Accuracy	**86.5%**

Notes: Cutpoint of p=0.5 was selected for classification

Table 17.1 Classification Table Based on Group 2 LR

		Observed		Total
	Predicted	0	1	
	0	93	7	100
	1	4	96	100
	Total	97	103	200
Sensitivity	**93.2%**	Specificity	**95.9%**	Accuracy	**94.5%**

Notes: Cutpoint of p=0.5 was selected for classification

Table 17.2 Classification Table Based on Group 2 GWLR

		Observed		Total
	Predicted	0	1	
	0	96	4	100
	1	2	98	100
	Total	98	102	200
Sensitivity	**96.1%**	Specificity	**98.0%**	Accuracy	**97.0%**

Notes: Cutpoint of p=0.5 was selected for classification

Table 18.1 Classification Table Based on Group 3 LR

		Observed		Total
	Predicted	0	1	
	0	86	14	100
	1	20	80	100
	Total	106	94	200
Sensitivity	**85.1%**	Specificity	**81.1%**	Accuracy	**83.0%**

Notes: Cutpoint of p=0.5 was selected for classification

Table 18.2 Classification Table Based on Group 3 GWLR

		Observed		Total
	Predicted	0	1	
	0	87	13	100
	1	8	92	100
	Total	95	105	200
Sensitivity	**87.6%**	Specificity	**91.6%**	Accuracy	**89.5%**

Notes: Cutpoint of p=0.5 was selected for classification

Table 19.1 Classification Table Based on Group 4 LR

		Observed		Total	
	Predicted	0	1		
	0	60	15	75	
	1	14	61	75	
	Total	74	76	150	
Sensitivity	**80.3%**	Specificity	**81.1%**	Accuracy	**80.7%**

Notes: Cutpoint of p=0.5 was selected for classification

Table 19.2 Classification Table Based on Group 4 GWLR

		Observed		Total	
	Predicted	0	1		
	0	65	10	75	
	1	12	63	75	
	Total	77	73	150	
Sensitivity	**86.3%**	Specificity	**84.4%**	Accuracy	**85.3%**

Notes: Cutpoint of p=0.5 was selected for classification

CHAPTER 4: DISCUSSION

A comparative analysis was performed in this study to assess the results of global and local logistic regression modeling. 85 candidate predictor variables were analyzed to discover relationships between environmental factors and landslide occurrence. Logistic regression (LR) was chosen for this research, because it is often counted among the most popular approaches for landslide susceptibility mapping (Guzzetti, Carrara, Cardinali, & Reichenbach, 1999). Traditional logistic regression modeling was compared to a more advanced technique, geographically weighted logistic regression (GWLR), that has been successfully used in other fields of science. GWLR is appropriate for datasets with great spatial variability, because it accounts for the spatial non-stationarity that is evident in most environmental data and produces more reliable results. For landslide hazard analysis, however, GWR has only been applied in a small number of studies (Chalkias, Kalogirou, & Ferentinou, 2011; Erener & Düzgün, 2010; Sabokbar, Roodposhti, & Tazik, 2014). None the less, these studies concluded that geographically weighted approaches provided more realistic predictions and offered greater spatial detail. It not only allowed for better interpretations of modeling estimates, but also improved the understanding of the role of local contributors. Regression outputs for the analysis conducted in this study confirmed such conclusions.

The models in this study captured several physical landslide processes. Many of the predictor variables that were found to be significant, have also been identified as vital components in other landslide research. Especially the role of slope, erosion potential, hydrologic groups, and geologic parent material on landslide susceptibility was consistent with the scientific literature. In all 5 models, the predictor slope had a positive parameter estimate which suggests that landslide susceptibility increases as slope increases. As slope gradients become steeper, shear stress on the parent material increases and greater resisting forces are necessary to prevent failure. This positive relationship is commonly observed in landslide susceptibility models. Furthermore, the parameter estimates for erosion potential were consistent across all models. Estimates were positive for severe erosion potential, and negative for slight erosion potential. This denotes that slopes with easily detachable soils are more prone to landslide activity. As the factor of soil erodibility, increases, removal of lateral support during heavy rain or snowmelt events becomes more likely. Soils with large k-factors,

such as silts, have higher risks for lateral or underlying support removal. Soil erodibility also plays an important role when analyzing hydrologic soil groups. Hydrologic Group D was included in two of the five regions and exhibited a positive parameter estimate. This result is consistent with the underlying mechanics of landslide activity. Since soils in group D have the greatest runoff and swelling potential, due to their large clay content, when adequately hydrated, clay rich soils expand and significantly increases lateral pressure. Enhanced shear stress contributes to slope instability and may result in slope failure. A similar process can also be observed in ultisols which have a clay-rich subsurface horizon. Finally, model results indicated that volcanic and sedimentary parent material contributed to the landslide hazard. Depending on the region, landslide susceptibility increased as these geologic classes increased. Deeply weathered siltstone and sandstone along Oregon's Coastal Range are often associated with creep and earthflow activity. In addition, volcanic material is prone to landslide activity because it has low internal cohesion when weathered.

Sensitivity and specificity computations verified that GWLR models were more accurate in predicting landslide and non-landslide events than standard logistic regression. Geographically weighted regressions improved accuracy by a range of 2.5% for sub region 2 to 9.5% for group 1. This suggests that GWLR models provided a better fit for data used in this study and improved the accuracy of the models. In addition, the variance of parameter estimates between sub regions indicated that the segmentation of data into sub regions was well rationalized. The magnitude of parameter estimates, as well as the selection of predictor variables used for each model, varied substantially across groups. Group models performed better than the global GWLR which also supports grouping of data into sub regions. Calibrating the grouping analysis and improving on the segmentation of data could further improve modeling results greatly. For example, by computing more precise inter-point distances, the sub regions could be adjusted for a more natural grouping. This would lower the GWR bandwidth and enhance model results.

Besides significant improvements in AIC and other modeling diagnostics, GWLR provided a more detailed output. Results for the variable slope (Figures 19–23) suggest that parameter estimates are not stationary across the study region. Instead, results vary significantly for various parts of western Oregon. For group 3, slope parameter estimates range from 0.170 to 0.534. This denotes that model estimates can deviate substantially for

different locations. An examination of predictor influence across the study region would not be possible with standard logistic regression. By applying a GWR, it is possible to interpret these results and, subsequently, recalibrate the model or the grouping of data to account for spatial patterns in the predictors. Similarly, parameter significance is dynamic across space. While global logistic models suggested that the explanatory variable slope was significant at the 95% confidence level for all sub regions, an examination of the geographically weighted regression results revealed that this was not the case for all regions. While the parameter is highly significant in most parts of the study area, there are also parts were slope is not a significant predictor. Especially in groups 1 and 2, the spatial difference of predictor significance is noticeable. This kind of information is lost when a traditional global logistic regression model is applied.

Even though GWR presented many advantages over traditional logistic regression modeling for the data used in this study, there are several limitations that must be addressed. First, the distribution of parameter estimates may be a result of model misspecification (Fotheringham, Brunsdon, & Charlton, 2002). Second, it has been noted that multicollinearity issues among local regression coefficients may invalidate any interpretation of the parameter estimates (Wheeler & Tiefelsdorf. 2005). Without applying standard diagnostic techniques, it is possible to encounter local collinearity even if the predictor variables are independent. Third, GWR is limited by the edge effect. Coastal landslide locations, for example, do not have the full 360-degree influence as landslides in the interior. Even though an adaptive kernel minimizes this problem, it is still important to note that the edge effect can bias parameter estimates. Finally, GWR addresses some of the non-stationarity in environmental data, but it does not explicitly model covariance. For that reason, researchers must apply caution and utilize diagnostic techniques to assure that parameter estimates can be interpreted accurately.

The modeling results for this analysis confirmed that GWLR models are a suitable alternative to standard logistic regression approaches. Traditional landslide research has not yet incorporated geographically weighted regression for hazard mapping. There is only a limited number of landslide studies that utilize this technique. Even though these studies confirmed the utility of GWR, which is also demonstrated in this analysis, it has not yet achieved broad acceptance in the field of landslide susceptibility analysis. In part, this can be

attributed to the innovative nature of this approach, and the fact that most statistical packages and mapping software do not incorporate geographically weighted regression. However, it is likely that future releases will include GWLR due to the rising popularity of the approach.

By considering the spatial correlation among regression parameters, the explanatory power of models increases. Since landslide research relies on the accuracy and reliability of predictions, improved models enhance the utility of susceptibility analyses. Constant evaluation of new approaches is necessary to assure that the field of hazard research utilizes the most innovative and appropriate techniques for a given objective. Only under these circumstances, it is possible for decision-makers to effectively mitigate the effects of slope failure and protect the population. In view of climatic changes that affect the frequency and distribution of landslide events, more localized models that account for the spatial variability are needed to predict slope failures effectively. The level of detail that is produced by GWLR models allows us to study the influence of predictors at the local level and analyze how independent variables change across space. This knowledge is invaluable for thorough landslide analysis. It gives researchers the opportunity to examine the underlying relationships that influence landslide susceptibility at the local level.

CHAPTER 5: LIMITATIONS AND FUTURE RESEARCH

Even though quality issues in the landslide inventory had created some conflicting results among climate predictors, overall, GWLR models presented an improvement compared to standard logistic regression. Inconsistent recording of landslide dates made recreating past climate conditions around the date of failure a challenging task. Clear weather drivers could only be identified in Group 3, where precipitation anomalies for winter landslides between November and March spiked significantly 4 days before the failure. However, since other sub regions lacked any significant relationships between weather drivers and landslide occurrence, parameter estimates for temperature and precipitation may not be accurate. To improve these predictors, it would be necessary to build independent models for different time periods. This would account for the seasonality in the landslide data. In addition, future research should incorporate a close examination of the landslide inventory to assure that recorded dates coincide with the date of failure and not the day of discovery. Moreover, the approach for extracting climate data at non-landslide locations also needs to be updated. Instead of assigning a random date using a uniform distribution, non-landslide dates should be computed by analyzing the temporal distribution of landslide events. This means that a higher frequency of winter landslides in the inventory must be reflected by the non-landslide date attribute as well. Modeling predictions could be significantly enhanced if not only spatial variation was considered, but also temporal variability.

Due to the high frequency of landslide events during the summer months, it is also advisable to investigate seismic predictor importance in future modeling efforts. As explained previously, a large number of slope failures occurred in August, the driest month of the year. Therefore, it is important to consider additional independent variables such as distance to fault lines, for example, to assure that no significant predictors are omitted from the analysis. Seismic data was not incorporated in this study because of its complexity at regional scales. However, for smaller study areas it is feasible to obtain geospatial data for tectonic uplift, volcanic eruptions, and other seismic activity efficiently.

The use of improved vegetation products could also enhance model accuracy. Since landcover is dynamic, it is proposed to utilize remotely sensed data to compute vegetation indices for a given time period. First, this would replace categorical landcover data with a

continuous measure of vegetation cover. For logistic regression with a limited number of landslide events, this would reduce the problem of separation and enhance quality of predictions. Second, by computing vegetation indices for several temporal ranges, it may be possible to evaluate the effects of landcover change on the distribution of slope failures. Geographically weighted modeling outputs would, consequently, not only account for spatial non-stationarity, but also address temporal variability.

REFERENCES

Abatzoglou, J. T. (2013). Development of gridded surface meteorological data for ecological applications and modelling. *International Journal of Climatology, 33*(1), 121-131.

Abatzoglou, J. T., Rupp, D. E., & Mote, P. W. (2014). Seasonal climate variability and change in the Pacific Northwest of the United States. *Journal of Climate, 27*(5), 2125-2142.

Baeza, C., & Corominas, J. (2001). Assessment of shallow landslide susceptibility by means of multivariate statistical techniques. *Earth surface processes and landforms, 26*(12), 1251-1263.

Bonnard, C. H., Tacher, L., & Beniston, M. (2008). Prediction of landslide movements caused by climate change: modelling the behaviour of a mean elevation large slide in the Alps and assessing its uncertainties. In Z. Chen, J. Zhang, K. Ho, F. Wu, & Z. Li (Eds.), *Landslides and Engineered Slopes* (pp. 217-227). London: Taylor & Francis Group.

Burns, W. J., & Watzig, R. J. (2014). *Statewide Landslide Information Database for Oregon: Release 3.0.* Portland, OR: Oregon Department of Geology and Mineral Industries.

Burns, W. J., Madin, I. P., & Ma, L. (2008). *Statewide Landslide Information Database for Oregon (SLIDO), Release 1.* Portland, OR: Oregon Department of Geology and Mineral Industries.

Caine, N. (1980). The rainfall intensity: duration control of shallow landslides and debris flows. *Geografiska Annaler. Series A. Physical Geography,* 23-27.

Campbell, R. H. (1973). *Isopleth map of landslide deposits, Point Dume quadrangle, Los Angeles County, California; an experiment in generalizing and quantifying areal distribution of landslides.* No. 535 United States Geological Survey.

Cardinali, M., Galli, M., Guzzetti, F., Ardizzone, F., Reichenbach, P., & Bartoccini, P. (2006). Rainfall induced landslides in December 2004 in south-western Umbria, central Italy: types, extent, damage and risk assessment. *Natural Hazards and Earth System Science, 6*(2), 237-260.

Carrara, A. (1983). Multivariate models for landslide hazard evaluation. *Journal of the International Association for Mathematical Geology, 15*(3), 403-426.

Carrara, A., Cardinali, M., Detti, R., Guzzetti, F., Pasqui, V., & Reichenbach, P. (1991). GIS techniques and statistical models in evaluating landslide hazard. *Earth surface processes and landforms, 16*(5), 427-445.

Chalkias, C., Kalogirou, S., & Ferentinou, M. (2011). Global and local statistical modeling for landslide susceptibility assessment, a comparative analysis. *17th ECQTG, 25.* Athens, Greece.

Clark, G. M. (2010). Changes in patterns of streamflow from unregulated watersheds in Idaho, Western Wyoming, and Northern Nevada. *Journal of the American Water Resources Association, 46*(3), 486-497.

Crozier, M. J. (1999). Prediction of rainfall-triggered landslides: A test of the antecedent water status model. *Earth surface processes and landforms, 24*(9), 825-833.

Cruden, D. M. (1991). A simple definition of a landslide. *Bulletin of Engineering Geology and the Environment, 43*(1), 27-29. doi:10.1007/BF02590167

Cruden, D. M., & Varnes, D. J. (1996). Landslide Types and Processes. In A. K. Turner, & R. L. Schuster (Eds.), *Landslides: investigation and mitigation.* Washington, D.C.: National Academy Press.

Dahal, R. K., & Hasegawa, S. (2008). Representative rainfall thresholds for landslides in the Nepal Himalaya. *Geomorphology, 100*(3), 429-443.

DeGraff, J. V. (1985). Using isopleth maps of landslide deposits as a tool in timber sale planning. *Environmental & Engineering Geoscience, 22*(4), 445-453.

Dhakal, A. S., & Sidle, R. C. (2004). Distributed simulations of landslides for different rainfall conditions. *Hydrological Processes, 18*(4), 757-776.

Erener, A., & Düzgün, H. (2010). Improvement of statistical landslide susceptibility mapping by using spatial and global regression methods in the case of More and Romsdal (Norway). *Landslides, 7*(1), 55-68.

Ermini, L., Catani, F., & Casagli, N. (2005). Artificial neural networks applied to landslide susceptibility assessment. *Geomorphology, 66*(1), 327-343.

FEMA. (1989). *Landslide Loss Reduction: A Guide for State and Local Government Planning.*

Fotheringham, A. S., Brunsdon, C., & Charlton, M. (2002). *Geographically Weighted Regression.* Wiley.

Geertsema, M., & Pojar, J. J. (2007). Influence of landslides on biophysical diversity—a perspective from British Columbia. *Geomorphology, 89*(1), 55-69. doi:10.1016/j.geomorph.2006.07.019

Glade, T., Crozier, M., & Smith, P. (2000). Applying probability determination to refine landslide-triggering rainfall thresholds using an empirical "Antecedent Daily Rainfall Model". *Pure and Applied Geophysics, 157*(6-8), 1059-1079.

Gökceoglu, C., & Aksoy, H. (1996). Landslide susceptibility mapping of the slopes in the residual soils of the Mengen region (Turkey) by deterministic stability analyses and image processing techniques. *Engineering Geology, 44*(1), 147-161.

Gorsevski, P. V., Gessler, P. E., Boll, J., Elliot, W. J., & Foltz, R. B. (2006). Spatially and temporally distributed modeling of landslide susceptibility. *Geomorphology, 80*(3), 178-198.

Gorsevski, P. V., Gessler, P. E., Foltz, R. B., & Elliot, W. J. (2006). Spatial prediction of landslide hazard using logistic regression and ROC analysis. *Transactions in GIS, 10*(3), 395-415.

Gorsevski, P. V., Jankowski, P., & Gessler, P. E. (2006). Heuristic approach for mapping landslide hazard integrating fuzzy logic with analytic hierarchy process. *Control and Cybernetics, 35*(1), 121-146.

Groisman, P. Y., Knight, R. W., Easterling, D. R., Karl, T. R., Hegerl, G. C., & Razuvaev, V. N. (2005). Trends in intense precipitation in the climate record. *Journal of Climate, 18*(9), 1326-1350.

Guzzetti, F., Carrara, A., Cardinali, M., & Reichenbach, P. (1999). Landslide hazard evaluation: a review of current techniques and their application in a multi-scale study, Central Italy. *Geomorphology, 31*(1), 181-216.

Guzzetti, F., Peruccacci, S., Rossi, M., & Stark, C. P. (2007). Rainfall thresholds for the initiation of landslides in central and southern Europe. *Meteorology and atmospheric physics, 98*(3-4), 239-267.

Hong, Y., Yu, G., & Wu, Y. (2011). Subterranean erosion in a crystalline schist landslide in Japan. *Environmental Earth Sciences, 64*(3), 685-691.

Hosmer, D., Lemeshow, S., & Sturdivant, R. (2013). *Applied Logistic Regression* (3rd ed.). Chicester: Wiley.

Hutchinson, J. N. (1988). General report: morphological and geotechnical parameters of landslides in relation to geology and hydrogeology. *International Journal of Rock Mechanics and Mining Sciences & Geomechanics Abstracts, 26*(2), 88.

Karl, T. R., & Knight, R. W. (1998). Secular trends of precipitation amount, frequency, and intensity in the United States. *Bulletin of the American Meteorological Society, 79*(2), 231-241.

Keefer, D. (1984). Landslides caused by earthquakes. *Geological Society of America Bulletin, 95*(4), 406-421.

Krejčí, O., Baroň, I., Bıl, M., Hubatka, F., Jurová, Z., & Kirchner, K. (2002). Slope movements in the Flysch Carpathians of Eastern Czech Republic triggered by extreme rainfalls in 1997: a case study. *Physics and Chemistry of the Earth, Parts A/B/C, 27*(36), 1567-1576.

Lee, S., Won, J. S., Jeon, S. W., Park, I., & Lee, M. J. (2015). Spatial landslide hazard prediction using rainfall probability and a logistic regression model. *Mathematical Geosciences, 47*(5), 565-589.

Miles, E. L., Snover, A. K., Hamlet, A. F., Callahan, B., & Fluharty, D. (2000). Pacific Northwest Regional Assessment: The Impacts of Climate Variability and Climate Change on the Water Resources of the Columbia River Basin. *Journal of the American Water Resources Association, 36*(2), 399-420.

Mote, P. W., & Salathe, E. P. (2010). Future climate in the Pacific Northwest. *Climatic Change, 100*(1-2), 29-50.

O'Connor, J. E., Hardison, J. H., & Costa, J. E. (2001). Debris flows from failures of Neoglacial-Age moraine dams in the Three Sisters and Mount Jefferson wilderness areas, Oregon. *US Geological Survey Professional Paper, 1606*, 1-93.

Ohlmacher, G. (2007). Plan curvature and landslide probability in regions dominated by earth flows and earth slides. *Engineering Geology, 91*(2), 117-134.

Price, M. F., & Butt, N. (Eds.). (2000). *Forests in sustainable mountain development: a state of knowledge report for 2000* (Vol. 5). CABI.

Restrepo, C., Walker, L. R., Shields, A. B., Bussmann, R., Claessens, L., Fisch, S., . . . Poveda, G. (2009). Landsliding and its multiscale influence on mountainscapes. *BioScience, 59*(8), 685-698. doi:10.1525/bio.2009.59.8.10

Sabokbar, H. F., Roodposhti, M. S., & Tazik, E. (2014). Landslide susceptibility mapping using geographically-weighted principal component. *Geomorphology, 226*, 15-24.

Sarkar, S., & Kanungo, D. P. (2004). An integrated approach for landslide susceptibility mapping using remote sensing and GIS. *Photogrammetric Engineering & Remote Sensing, 70*(5), 617-625.

Schulz, Galloway, & Higgins. (2012). Evidence for earthquake triggering of large landslides in coastal Oregon, USA. Geomorphology, 141-142, 88-98.

Sharpe, C. F. (1938). *Landslides and related phenomena: a study of mass-movements of soil and rock.* Pageant Books.

Sidle, R. C., & Ochiai, H. (2006). Landslides: processes, prediction, and land use. *American Geophysical Union, 18*, 1-312.

Smith, R. L., & Roe, W. P. (2015). *Readme File For Oregon Geologic Data Compilation (OGDC)-Release 6.* Portland: Oregon Department of Geology and Mineral Industries.

Soeters, R., & Van Westen, C. J. (1996). Slope instability recognition, analysis and zonation. In R. L. Schuster, & A. K. Turner (Eds.), *Landslides, investigation and mitigation* (pp. 129-177). Washington, D.C.: National Academy Press.

Stoffel, M., Tiranti, D., & Huggel, C. (2014). Climate change impacts on mass movements—case studies from the European Alps. *Science of the Total Environment, 493*, 1255-1266.

Swanson, F. J., & Swanston, D. (1977). Complex mass-movement terrains in the western Cascade Range, Oregon. *Reviews in Engineering Geology, 3*, 113-124.

Swanston, D. N. (1984). *Effect of geology on soil mass movement activity in the Pacific Northwest.* Pacific Northwest Forest and Range Experiment Station, Forestry Sciences Laboratory.

Swanston, D., & Swanson, F. J. (1976). Timber harvesting, mass erosion, and steepland forest geomorphology in the Pacific Northwest. *Geomorphology and engineering*, 199-221.

Terlien, M. T., Van Westen, C. J., & Van Asch, T. W. (1995). Deterministic modelling in GIS-based landslide hazard assessment. In A. Carrara, & F. Guzzetti (Eds.), *Geographical information systems in assessing natural hazards* (pp. 57-77). New York: Springer.

Turner, A. K., & McGuffey, V. C. (1996). Organization of Investigation Process. In A. K. Turner, & R. L. Schuster (Eds.), *Landslides: Investigation and Mitigation.* Washington, D.C.: National Academy Press.

United States Geological Survey. (2013). LANDFIRE Existing Vegetation Type. Retrieved February 2016, from http://www.landfire.gov/index.php

United States Geological Survey. (2016). *3DEP products and services: The National Map, 3D Elevation Program*. Retrieved February 2016, from http://nationalmap.gov/3DEP/3dep_prodserv.html

USDA/NRCS. (2014). *Gridded Soil Survey Geographic (gSSURGO) Database.* United States Department of Agriculture.

Van Asch, T. W., Buma, J., & Van Beek, L. P. (1999). A view on some hydrological triggering systems in landslides. *Geomorphology, 30*(1), 25-32.

Varnes, D. J. (1978). Slope movement types and processes. In R. L. Schuster, & R. J. Krizek (Eds.), *Landslide Analysis and Control* (pp. 11-33). Washington, DC: Special Report 176: Transportation Research Board, National Research Council.

Varnes, D. J. (1984). *Landslide hazard zonation: a review of principles and practice* (Vol. 3). Paris: Unesco.

Westerling, A. L., Hidalgo, H. G., Cayan, D. R., & Swetnam, T. W. (2006). Warming and earlier spring increase western US forest wildfire activity. *Science, 313*(5789), 940-943.

Wheeler, D., &Tiefelsdorf, M. (2005). Multicollinearity and correlation among local regression coefficients in geographically weighted regression. Journal of Geographical Systems, 7(2), 161-187.

Wieczorek, G. F. (1996). Landslide Triggering Mechanisms. In A. K. Turner, & R. L. Schuster (Eds.), *Landslides: investigation and mitigation.* Washington, D.C.: National Academy Press.

Wright, R. H., Campbell, R. H., & Nilsen, T. H. (1974). Preparation and use of isopleth maps of landslide deposits. *Geology, 2*(10), 483-485.